

State Space Modeling of Neural Spike Train and Behavioral Data

6

Zhe Chen, Riccardo Barbieri, Emery N. Brown

Neuroscience Statistics Research Laboratory, Department of Brain and Cognitive Sciences, Massachusetts Institute of Technology, Cambridge, Massachusetts; Harvard-MIT Division of Health Sciences and Technology, Massachusetts Institute of Technology, Cambridge, Massachusetts; Massachusetts General Hospital, Harvard Medical School, Boston, Massachusetts

6.1 INTRODUCTION

State space modeling is an established framework for analyzing stochastic and deterministic dynamical systems that are measured or observed through a stochastic process. This highly flexible paradigm has been successfully applied in engineering, statistics, computer science, and economics to solve a broad range of dynamical systems problems (Mendel, 1995; Kitagawa and Gersh, 1996; Shephard and Pitt, 1997; Kim and Nelson, 1999; Durbin and Koopman, 2001). Other terms used to describe state space modeling are hidden Markov models (Cappé et al., 2005) and latent process models (Fahrmeir and Tutz, 2001). The most-studied state space modeling tool is the Kalman filter, which defines an optimal algorithm for analyzing linear Gaussian systems measured with Gaussian error (Mendel, 1995).

The revolution in neuroscience recording technologies in the last 20 years has provided many novel ways to study the dynamic activity of the brain and central nervous system. These technologies include multi-electrode recording arrays (Wilson and McNaughton, 1993, 1994), functional magnetic imaging (Kwong et al., 1992; Ogawa et al., 1992), electroencephalography and magnetoencephalography (Hämäläinen et al., 1993), diffuse optical tomography (Boas et al., 2001), calcium imaging (Denk et al., 1990), and behavioral data (Wirth et al., 2003). Because a fundamental feature of many neuroscience data analysis problems is that the underlying neural system is dynamic and is observed indirectly through measurements from one or a combination of these different recording modalities,

the state space paradigm provides an ideal framework for developing statistical tools to analyze neural data.

Neural spiking activity recorded from single or multiple electrodes is one of the principal types of data recorded in neurophysiological experiments. Because neural spike trains are time series of action potentials (i.e., all-or-nothing responses), point process theory has been shown to provide an accurate framework for modeling the stochastic structure of single and multiple neural spike trains (Brown et al., 2003, 2004; Brown, 2005). An important objective of these experiments is to study how neurons represent and transmit information in their ensemble spiking activity. In behavioral learning experiments, a frequently recorded type of data is time series of binary responses that track whether a subject responds correctly or incorrectly to a task across series of multiple presentations or trials (Jog et al., 1999; Wirth et al., 2003; Barnes et al., 2005; Law et al., 2005). Each binary measurement may be considered an observation of a Bernoulli random variable. The objective of the analysis is to determine how this Bernoulli probability changes as a function of repeated attempts at the task.

Both the neural spiking activity recorded from neurophysiological experiments and the binary responses recorded in learning experiments may be viewed as time series of 0–1 responses. Moreover, because the underlying systems being studied in neurophysiological and learning experiments are dynamic, these processes readily lend themselves to analysis using the state space paradigm. Point process measurements and binary observations are types of observation models not commonly studied in state space modeling. However, they are appropriate for two types of neuroscience data.

In this chapter, we discuss the application of the state space paradigm to the analysis of neural spike trains and behavioral learning data. We first define point process and binary observation models and review the framework for state space filtering and state space smoothing. To illustrate the state space paradigm we discuss four data analysis problems:

- Ensemble neural spike train decoding (Brown et al., 1998; Barbieri et al., 2004)
- Analysis of neural receptive field plasticity in one and two dimensions (Brown et al., 2001; Ergun et al., 2007)
- Dynamic analysis of individual and population behavioral learning (Smith and Brown, 2003; Smith et al., 2004)
- Estimation of cortical UP/DOWN states (Chen et al., 2009)

For each problem we describe the observation model, the state space model, and the estimation algorithm, and apply the paradigm in the analysis of actual data.

6.2 STATE SPACE MODELING PARADIGM

The state space model consists of two equations: the state equation and the observation equation. The state equation defines the temporal evolution of the state process as a dynamical system. The states can be described either in continuous time by a deterministic or stochastic differential equation, or in discrete time by a deterministic or stochastic difference equation. If the current state depends only on the previous state, the state space model is termed Markovian. The observation equation defines how the state is observed or measured. The observation model is generally stochastic, and the values of the observation process can be either continuous or discrete. In the analyses we present, the observation processes are discrete.

6.2.1 Notation

Because our objective is to analyze neural spike train and behavioral data, we assume that the observations are recorded from either a point process or a binary process. To define the point process we assume that we have an observation interval $(0, T]$ and that we divide it into subintervals of width Δ . We take x_t to be the value of the state process and y_t to be the observation recorded in the interval $[t, t + \Delta]$. A point process is a binary $(0 - 1)$ stochastic process defined in continuous time characterized by its conditional intensity function (CIF), $\lambda(t|x_t, H_t)$, where H_t represents the relevant history of the point process up to time t (Daley and Vere-Jones, 2002; Brown, 2005). The CIF defines the probability of observing an event from the point process in the interval $[t, t + \Delta]$ as $\Pr(y_t = 1|x_t, H_t) = \lambda(t|x_t, H_t)\Delta + o(\Delta)$. That is, as Δ becomes small, the probability of more than one event in the interval $[t, t + \Delta]$ tends to 0. The CIF is a history-dependent generalization of the rate function of a Poisson process. The point process models are used to analyze neural spiking activity.

To define the discrete binary process we assume that in the interval $(0, T]$ there is a set of lattice points $t = 1, 2, \dots, T$. We let y_t denote the discrete binary observation and x_t denote the state process at time t . The discrete binary process is a $(0 - 1)$ stochastic process recorded in discrete time defined by the probability of observing an event as $\Pr(y_t = 1|x_t) = p_t$, for $t = 1, \dots, T$ (Fahrmeir and Tutz, 2001; Smith and Brown, 2003). We use the discrete

binary process to model the binary responses recorded in learning experiments. For both the point process and the discrete binary process, we take $y_{0:t} = (y_1, \dots, y_t)$ to be the data recorded in $(0, t]$ for $t = 1, \dots, T$.

6.2.2 Recursive Form of Bayes' Rule

The objective of state space modeling is to compute the optimal estimate of the state given the observed data. There are two important cases that are typically considered. To state them we consider $y_{0:s}$ for $s = 1, \dots, T$. If we take $s = t$ and we wish to determine the best estimate of the state x_t given the observation $y_{0:t}$, then we seek a solution to the filtering problem; if we take $s = T$ and we wish to determine the best estimate of the state x_t given the observation $y_{0:T}$, then we seek a solution to the smoothing problem.

To develop the state space analysis paradigm and make formal statements on the filtering and smoothing problems, we first derive a recursive form of Bayes' rule. The objective for the filtering problem is to compute at each time t the probability density of the state given the data. Because of the state space structure, this posterior density can be expressed in a recursive form as

$$\begin{aligned} p(x_t | y_{0:t}) &= \frac{p(x_t, y_{0:t})}{p(y_{0:t})} \\ &= \frac{p(x_t, y_{0:t} | y_{0:t-1}) p(y_{0:t-1})}{p(y_t | y_{0:t-1}) p(y_{0:t-1})} \\ &= \frac{p(x_t | y_{0:t-1}) p(y_{0:t} | x_t, y_{0:t-1})}{p(y_t | y_{0:t-1})} \\ &= \frac{p(x_t | y_{0:t-1}) p(y_t | x_t, y_{0:t-1})}{p(y_t | y_{0:t-1})} \end{aligned} \quad (6.1)$$

where the Chapman-Kolmogorov, or one-step prediction, equation is

$$p(x_t | y_{0:t-1}) = \int p(x_t | x_{t-1}) p(x_{t-1} | y_{0:t-1}) dx_{t-1} \quad (6.2)$$

and the normalizing constant is

$$p(y_t | y_{0:t-1}) = \int p(x_t | y_{0:t-1}) p(y_t | x_t, y_{0:t-1}) dx_t \quad (6.3)$$

where $p(y_t | x_t, y_{0:t-1})$ is the observation equation and $p(x_t | x_{t-1})$ is the state equation in the state space model. The posterior probability density (Eq. (6.1)) and the Chapman-Kolmogorov equation (Eq. (6.2)) constitute the

recursive form of Bayes' rule. Equations (6.1) and (6.2) provide the fundamental relations to develop our state space analyses for point process and binary observations. These two equations are used to derive the Kalman filter (Haykin, 2002), conduct time series analyses with smoothness priors (Kitagawa and Gersh, 1996; Durbin and Koopman, 2001), design dynamic generalized linear models (Fahrmeir and Tutz, 2001), and build particle filters (Doucet et al., 2001).

To solve the smoothing problem, we are interested in computing the posterior density of the state x_t given all of the observed data $y_{0:T}$. We can express the smoothing probability density in terms of the filtering probability density as follows:

$$\begin{aligned} p(x_t | y_{0:T}) &= \int p(x_t, x_{t+1} | y_{0:T}) dx_{t+1} \\ &= \int p(x_{t+1} | y_{0:T}) p(x_t | x_{t+1}, y_{0:T}) dx_{t+1} \\ &= \int p(x_{t+1} | y_{0:T}) p(x_t | x_{t+1}, y_{0:t}) dx_{t+1}, \\ &= p(x_t | y_{0:t}) \int p(x_{t+1} | y_{0:T}) p(x_{t+1} | x_t, y_{0:t}) dx_{t+1} \\ &= p(x_t | y_{0:t}) \int \frac{p(x_{t+1} | y_{0:T}) p(x_{t+1} | x_t)}{p(x_{t+1} | y_{0:T})} dx_{t+1} \end{aligned} \quad (6.4)$$

If the observation equation is linear and Gaussian and the state equation is linear and Gaussian, or if Gaussian approximations have been used to estimate the filtering probability density, then the solution to the smoothing probability density is Gaussian and its mean and variance can be computed recursively by the fixed-interval smoothing algorithm (Fahrmeir and Tutz, 2001).

6.2.3 Classes of Filtering and Smoothing Problems

Applying Eqs. (6.1), (6.2), and (6.4) to actual data analyses requires that a statistical model be defined for each problem. This model will have a set of parameters θ , which must be estimated from either current or previous data. We can use θ to parameterize the state equation, the observation equation, or both. For both the filtering and smoothing problems, θ can be either known or estimated and either static or dynamic. We then define our applications of the state space paradigm in terms of different classes of filtering and smoothing problems by expressing Eqs. (6.1), (6.2), and (6.4) as functions of θ . The three classes of filtering and smoothing problems we consider are state space filtering with a known or estimated static parameter θ , $p(x_t | y_{0:t}, \theta)$; state

space filtering with an estimated dynamic parameter θ_t , $p(x_t|y_{0:t}, \theta_t)$; and state space smoothing with an estimated static parameter θ , $p(x_t|y_{0:T}, \theta)$. A third problem is one of prediction, in which we consider $p(x_t|y_{0:T}, \theta)$ where $t > T$. This problem arises naturally in the design of algorithms for brain-computer interfaces (Serruya et al., 2002; Taylor et al., 2002; Musallam et al., 2004; Hochberg et al., 2006; Santhanam et al., 2006).

6.3 APPLICATIONS OF THE STATE SPACE PARADIGM IN NEUROSCIENCE DATA ANALYSIS

The following sections discuss how the state space paradigm is applied in neuroscientific data analysis.

6.3.1 Neural Spike Train Decoding and Point Process Filter Algorithms

The development of multiple electrode arrays allows neuroscientists to record the simultaneous spiking activity of large numbers of neurons. For example, the technical capability to record the spiking activity of large numbers of hippocampal place cells—between 20 and 100—along with a rat's position in its environment has made feasible a formal quantitative study of how rats encode spatial information in short-term memory and use it for navigation. Investigation of these questions requires statistical methods to analyze how the animal's position in the environment (the continuous stimulus) is represented in the firing patterns of place cells (multidimensional point processes).

The mathematical techniques used in neuroscience to study how spike train firing patterns represent biological signals and external stimuli are termed neural decoding algorithms (Rieke et al., 1997; Brown et al., 1998; Barbieri et al., 2004; Eden et al., 2004; Wu et al., 2006, 2009). Many data analyses of population coding have used decoding algorithms. Examples include position representation by ensembles of rat hippocampal neurons (Brown et al., 1998; Zhang et al., 1998), velocity encoding by fly H1 neurons (Bialek et al., 1991), velocity and position encoding by M1 neurons (Shoham et al., 2005; Truccolo et al., 2005), and natural scene representations by catLGN neurons (Stanley et al., 1999). How to develop optimal strategies for constructing and testing decoding algorithms is an important question in computational neuroscience. The decoding analysis proceeds typically in two stages: encoding and decoding. In the encoding stage, neural spiking activity is characterized as a function of the biological signal (Figure 6.1(a)). In the decoding stage, the relation is inverted and the signal is estimated from the spiking activity of

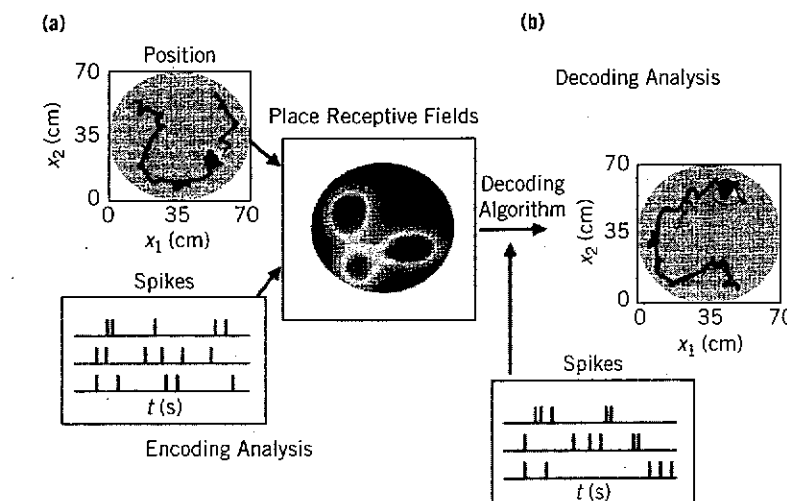


FIGURE 6.1

Decoding of position from ensemble rat neural spiking activity. (a) Encoding analysis: The relation between the biological stimulus (trajectory of the rat in the environment, solid black line in the Position panel) and spiking activity (Spikes panel) is estimated as place receptive fields for three neurons. (b) Decoding analysis: The estimated place receptive fields are used in a Bayesian decoding algorithm to compute the predicted position (thin black line) of the rat in the environment from new spiking activity of the neural ensemble recording during the decoding stage. The predicted position is compared to the observed position (thick black line) during the decoding stage. The oval outline defines a 95% confidence region centered at that location. Please see this figure in color at the companion web site: www.elsevierdirect.com/companions/9780123750273

Source: Brown et al. (2004), *Nature Neuroscience*, reprinted with permission.

the neurons (Figure 6.1(b)). The state space framework provides a systematic means of formulating the decoding problem.

To illustrate the application of a state space model to the neural spike trains decoding problem, we assume that we observe the simultaneous neural spiking activity of C hippocampal neurons of a rat foraging in an open circular environment (Brown et al., 1998; Barbieri et al., 2004). During the decoding interval $(0, T^d]$, we record the spiking activity of C neurons. For $c = 1, \dots, C$ and $t \in (0, T^d]$, let y_t^c be 1 if there is a spike in the interval $[t, t + \Delta]$ from neuron c and 0 otherwise; let $y_t = \{y_t^1, \dots, y_t^C\}$ be the set of observations in $[t, t + \Delta]$ from the C neurons. Also, let $y_{0:t}^c = \{y_{0:t}^1, y_{0:t}^2, \dots, y_{0:t}^C\}$ be the spiking activity from neuron c and $y_{0:t} = \{y_{0:t}^1, \dots, y_{0:t}^C\}$ be the ensemble spiking activity in $(0, t]$. The state is the animal's position in two dimensions $x_t = (x_{1,t}, x_{2,t})$. The CIF for neuron c is $\lambda(x_t|y_{0:t-1}, \theta^c)$, where θ^c is a parameter that depends on the equation being used to model the place receptive field.

For a small Δ , under the assumption that the spiking activity of the neurons in the ensemble is conditionally independent, the joint probability density or observation model for the interval $[t, t + \Delta]$ is as follows (Brown et al., 1998; Smith and Brown, 2003):

$$\begin{aligned} p(y_t|x_t, y_{0:t-1}, \theta) &= \prod_{c=1}^C p(y_t^c|x_t, y_{0:t-1}, \theta^c) \\ &= \exp \left[\sum_{c=1}^C y_t^c \log \lambda^c(x_t|y_{0:t-1}, \theta^c) - \sum_{c=1}^C \lambda^c(x_t|y_{0:t-1}, \theta^c) \Delta \right] \end{aligned} \quad (6.5)$$

where $\theta = \{\theta^1, \dots, \theta^C\}$. Conditional independence means that neurons are only related through the dynamics of the state variable.

Analysis of the decoding problem without satisfying this assumption requires a network likelihood model, such as the one used in Okatan et al. (2005) to model dependence among the neurons not related to the state variable. We do not consider this problem. Here, the state equation for x_t is the first-order auto-regressive model

$$x_t = Fx_{t-1} + v_t \quad (6.6)$$

where v_t is independent two-dimensional Gaussian noise with zero mean and covariance matrix Σ_v . The CIF model of the receptive field of neuron c is either the Gaussian function (Brown et al., 1998):

$$\lambda(x_t, \theta^c) = \exp \left\{ \alpha^c - \frac{1}{2}(x_t - \mu^c)(W^c)^{-1}(x_t - \mu^c) \right\} \quad (6.7)$$

where $\theta^c = (\alpha^c, \mu^c, W^c)$, or the log linear function defined by

$$\lambda(x_t, \theta^c) = \exp \left\{ \sum_{j=1}^J \theta_j^c z_j(x_t) \right\} \quad (6.8)$$

where the z_j are Zernike polynomials—that is, orthogonal polynomials on a unit disk (Barbieri et al., 2004).

To evaluate the system in Eqs. (6.1) and (6.2), as related to the model in Eqs. (6.5) and (6.6), we apply the *maximum a posteriori* (MAP) derivation of the Kalman filter and approximate $p(x_t|y_{1:t})$ as Gaussian probability densities

6.3 Applications of the State Space Paradigm in Neuroscience

by recursively computing their means (modes) and negative inverse of the Hessian matrices (covariance matrices) (Mendel, 1995; Brown et al., 1998). To initiate the recursive algorithm, let the notation $t|j$ denote the expectation of the state variable at t given the responses up to time j . We assume that the mean $x_{t-1|t-1}$ and covariance matrix $W_{t-1|t-1}$ have been estimated at time $t - 1$. That is, we take $p(x_{t-1}|y_{0:t-1})$, the posterior probability density at time $t - 1$, to be the Gaussian probability density with mean $x_{t-1|t-1}$ and covariance matrix $W_{t-1|t-1}$. The next step is to compute $p(x_t|y_{0:t-1})$, the one-step prediction probability density at time t . This is the probability density of the predicted position at t given the spiking activity in $(0, t - 1]$. It follows from standard properties of integrals of Gaussian functions that the mean and covariance matrix are respectively defined as

$$x_{t|t-1} = E(x_t|y_{0:t}) = \mu_x + Fx_{t-1|t-1} \quad (6.9)$$

$$W_{t|t-1} = \text{Var}(x_t|y_{0:t}) = FW_{t-1|t-1}F' + RW_\varepsilon \quad (6.10)$$

which correspond, respectively, to the one-step prediction estimate and the one-step prediction variance. Assuming a Gaussian approximation, we have

$$p(x_t|y_{0:t-1}) = (2\pi)^{-1} |W_{t|t-1}|^{-\frac{1}{2}} \exp \left\{ -\frac{1}{2}(x_t - x_{t|t-1})' W_{t|t-1}^{-1} (x_t - x_{t|t-1}) \right\}. \quad (6.11)$$

Substituting Eqs. (6.5) and (6.11) into Eq. (6.1), and neglecting the denominator and other terms that do not depend on position, we obtain an explicit expression for the probability density of position at time t given the spiking activity in $(0, t]$:

$$\begin{aligned} p(x_t|y_{0:t}) &\propto \exp \left\{ -\frac{1}{2}(x_t - x_{t|t-1})' W_{t|t-1}^{-1} (x_t - x_{t|t-1}) \right\} \\ &\times \exp \left[\sum_{c=1}^C y_t^c \log \lambda^c(x_t|y_{0:t-1}) - \sum_{c=1}^C \lambda^c(x_t|y_{0:t-1}) \Delta \right]. \end{aligned} \quad (6.12)$$

To evaluate Eq. (6.12), we further assume a Gaussian approximation by deriving a quadratic approximation to $\log p(x_t|y_{0:t})$. Thus, we rewrite Eq. (6.1) as

$$p(x_t|y_{0:t}) \propto p(x_t|y_{0:t-1})p(y_t|x_t). \quad (6.13)$$

Given $p(x_t|y_{0:t})$, the MAP estimate of x_t is

$$\hat{x}_t = \arg \max p(x_t|y_{0:t}). \quad (6.14)$$

Simply stated, the MAP estimate is the mode of the posterior density. Given a posterior probability density $p(x_t|y_{0:t})$ and \hat{x}_t , an approximate MAP estimate of x_t , we can expand the log posterior probability density in a Taylor series around \hat{x}_t to obtain

$$\begin{aligned} \log p(x_t|y_{0:t}) &= \log p(\hat{x}_t|y_{0:t}) + \nabla \log p(\hat{x}_t|y_{0:t})(x_t - \hat{x}_t) \\ &\quad + \frac{1}{2}(x_t - \hat{x}_t)' \nabla^2 \log p(\hat{x}_t|y_{0:t})(x_t - \hat{x}_t) + \dots \\ &\approx \log p(\hat{x}_t|y_{0:t}) + \frac{1}{2}(x_t - \hat{x}_t)' \nabla^2 \log p(\hat{x}_t|y_{0:t})(x_t - \hat{x}_t) \end{aligned}$$

because $\nabla \log p(\hat{x}_t|y_{0:t}) = 0$ by definition of the MAP estimate. Hence,

$$p(x_t|y_{0:t}) \approx p(\hat{x}_t|y_{0:t}) \exp \left\{ \frac{1}{2}(x_t - \hat{x}_t)' \nabla^2 \log p(\hat{x}_t|y_{0:t})(x_t - \hat{x}_t) \right\}. \quad (6.15)$$

gives the Gaussian approximation to a posterior of probability density defined as

$$p(x_t|y_{0:t}) \approx N(\hat{x}_t, W_{t|t}) \quad (6.16)$$

where \hat{x}_t is the posterior mode (the MAP estimate of x_t) in Eq. (6.15) and

$$W_{t|t} = -[\nabla^2 \log p(\hat{x}_t|y_{0:t})]^{-1}. \quad (6.17)$$

In our example, from Eq. (6.12), the log posterior $\log p(x_t|y_{0:t})$ is

$$\begin{aligned} \log p(x_t|y_{0:t}) &\propto -\frac{1}{2}(x_t - x_{t|t-1})' W_{t|t-1} (x_t - x_{t|t-1}) \\ &\quad + \sum_{c=1}^C y_{t-1,c}^c \log \lambda^c(x_t|y_{0:t-1}) - \sum_{c=1}^C \lambda^c(x_t|y_{0:t-1}) \Delta. \quad (6.18) \end{aligned}$$

The gradient and the Hessian matrix required for the quadratic approximation are given respectively by

$$\begin{aligned} \nabla \log p(x_t|y_{0:t}) &= -W_{t|t-1}^{-1}(x_t - x_{t|t-1}) \\ &\quad + \sum_{c=1}^C \nabla \log \lambda^c(x_t|y_{0:t-1}) [y_{t-1,c}^c - \lambda^c(x_t|y_{0:t-1}) \Delta] \end{aligned} \quad (6.19)$$

$$\begin{aligned} \nabla^2 \log p(x_t|y_{0:t}) &= -W_{t|t-1}^{-1} + \sum_{c=1}^C \nabla^2 \log \lambda^c(x_t|y_{0:t-1}) [y_t^c - \lambda^c(x_t|y_{0:t-1}) \Delta] \\ &\quad - \nabla \log \lambda^c(x_t|y_{0:t-1}) [\nabla \lambda^c(x_t|y_{0:t-1}) \Delta]' \end{aligned} \quad (6.20)$$

Solving for x_t in Eq. (6.19) yields the posterior mode, and taking the negative inverse of the Hessian from Eq. (6.20) yields the covariance matrix. We term the resulting recursive algorithm the point process filter algorithm (Brown et al., 1998; Barbieri et al., 2004) and summarize it as follows:

- One-step prediction:

$$x_{t|t-1} = \mu_x + \hat{F} x_{t-1|t-1}, \quad (6.21)$$

- One-step prediction variance:

$$W_{t|t-1} = \hat{F} W_{t-1|t-1} \hat{F}' + R \hat{W}_e \quad (6.22)$$

- Posterior mode:

$$x_{t|t} = x_{t|t-1} + W_{t|t-1} \sum_{c=1}^C \nabla \log \lambda^c(x_{t|t}|\hat{\theta}_j^c) [y_t^c - \lambda^c(x_{t|t}|\hat{\theta}_j^c) \Delta] \quad (6.23)$$

- Posterior variance:

$$\begin{aligned} W_{t|t}^{-1} &= \left[W_{t|t-1}^{-1} - \sum_{c=1}^C \left[\nabla^2 \log \lambda^c(x_{t|t}|\hat{\theta}_j^c) [y_t^c - \lambda^c(x_{t|t}|\hat{\theta}_j^c) \Delta] \right. \right. \\ &\quad \left. \left. - \nabla \log \lambda^c(x_{t|t}|\hat{\theta}_j^c) [\nabla \lambda^c(x_{t|t}|\hat{\theta}_j^c) \Delta]' \right] \right] \end{aligned} \quad (6.24)$$

for $t = 1, \dots, T$, where $\lambda^c(x_{t|t}|\hat{\theta}_j^c)$ is the conditional intensity (rate) function for either the spatial Gaussian or Zernike model for neuron c ; $\hat{\theta}_j^c$ is the associated model parameter for either the spatial Gaussian ($j = G$) or Zernike ($j = Z$) model estimated from the encoding analysis; \hat{F} and \hat{W}_e are, respectively, the estimates of the transition matrix and the white noise covariance matrix for the AR(1) model from the encoding analysis; and R is a scale factor.

The two-dimensional position and the spiking activity of 32 (34) neurons recorded from two rats, animal 1 (2) for 23 (25) minutes, were analyzed. The encoding analysis was performed on the first 13 (15) minutes of ensemble neural spiking activity from animals 1 (2), during which the parameters of the Gaussian and Zernike place receptive field models, as well as the position model, were estimated for each neuron for both animals. The decoding algorithm was applied to the last 10 minutes for each. An example of one minute of the application of the decoding algorithm comparing the Gaussian and Zernike models is shown in Figure 6.2(a). The median error for each of the 15-second segments is smaller for the Zernike model than for the Gaussian model. In general, the Zernike model gave more accurate decoding results than the Gaussian model, as illustrated by the box plots of the error distributions in Figure 6.2(b). The median error for the Zernike (Gaussian) model was 5.9 and (7.9) for animal 1, and 5.5 and (7.7) for animal 2. For animal 1 the error distribution of the Zernike model lies to the left of the error distribution for the Gaussian model. Although for animal 2, the error distribution of the Zernike model lies to the left of the error distribution of the Gaussian model up to the 75th percentile, the Zernike model error distribution has a larger right tail. The analyses from both models demonstrate that the hippocampus maintains a dynamic representation of the animal's position in its environment as encoded in the ensemble spiking activity.

6.3.2 Neural Receptive Field Plasticity and Instantaneous Steepest Descent Filtering

The receptive fields of neurons are dynamic. That is, their responses to relevant stimuli change with experience. Experience-dependent change or plasticity has been documented in a number of brain regions. In the rat hippocampus, the pyramidal neurons in the CA1 region have spatial receptive fields. As a rat executes a behavioral task, a given CA1 neuron fires only in a restricted region of the experimental environment, termed the cell's spatial or place receptive field. Place fields change in a reliable manner as the animal executes its task. When the experimental environment is a linear track, these spatial receptive fields have been shown to migrate and skew in the direction opposite the cell's preferred direction of firing relative to

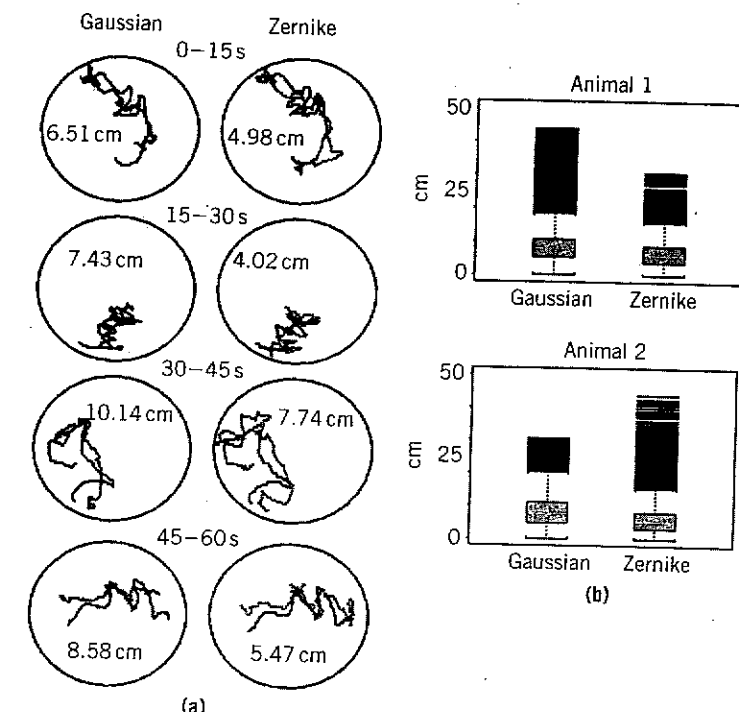


FIGURE 6.2

Decoding comparison and box plots of the error distributions for the 10 minutes of the decoding analysis. (a) Trajectory decoding comparison between two encoding models from 60s-recordings of one animal. (b) Box plot summaries of the decoding error (defined as $|\text{True Position} - \text{Estimated Position}|$) distributions for the spatial Gaussian model and the optimal Zernike polynomial. The lower border of the box is the 25th percentile of the distribution and the upper border is the 75th percentile. The white bar within the box is the median of distribution. The distance between the 25th and 75th percentiles is the interquartile range (IQR). The lower (upper) whisker is at $1.5 \times \text{IQR}$ below (above) the 25th (75th) percentile. All the black bars below (above) the lower (upper) whiskers are far outliers. For reference, less than 0.35% of the observations from a Gaussian distribution would lie beyond the 75th percentile plus $1.5 \times \text{IQR}$. Please see this figure in color at the companion web site: www.elsevierdirect.com/companions/9780123750273

Source: Barbieri et al. (2004), *Neural Computation*, Reprinted with permission, Copyright © 2004 MIT Press.

the animal's movement, and to increase in scale and maximum firing rate (Frank et al., 2004).

As an illustration of this behavior, an actual place cell spike train recorded from a rat running back and forth for 1200 s on a 300-cm U-shaped track is shown in Figure 6.3. To display all of the experimental data on a

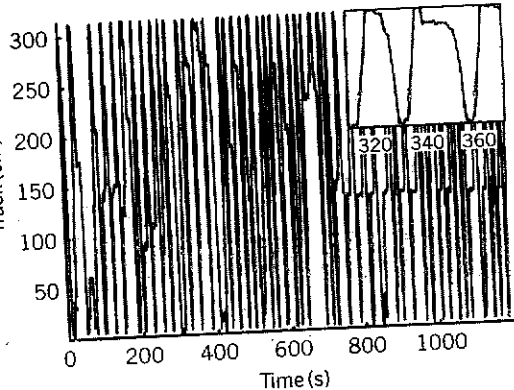


FIGURE 6.3

Place specific firing dynamics of an actual CA1 place cell recorded from a rat running back and forth on a 300-cm U-shaped track for 1200 s. The track was linearized to display the entire experiment in a single graph. The vertical lines show the animal's position and the light gray dots indicate the time at which a spike was recorded. The inset is an enlargement of the display from 320 to 360 s to show the cell's unidirectional firing—that is, spiking only when the animal runs from the bottom to the top of the track. Please see this figure in color at the companion web site: www.elsevierdirect.com/companions/9780123750273

Source: Brown et al. (2001). Proceedings of National Academy of Sciences, Reprinted with permission, copyright © 2001 National Academy of Science, U.S.A.

single graph, we represent the track linearly. The actual trajectory is irregular because the animal stops and starts several times and, in two instances (50 s and 650 s), turns around shortly after initiating its run. On several of the upward passes, particularly in the latter part of the experiment, the animal slows as it approaches the curve in the U-shaped track at approximately 150 cm. The strong place-specific firing of the neuron is readily visible because the spiking activity occurs almost exclusively between 50 and 100 cm. The spiking activity of the neuron is entirely unidirectional as the cell discharges only as the animal runs up and not down the track (Figure 6.3, inset).

Brown et al. (2001) proposed a state space model to analyze these data, in which the observation equation is

$$\Pr(y_t | \lambda(x_t, \theta_t)) = \exp(y_t \log \lambda(x_t, \theta_t) \Delta - \lambda(x_t, \theta_t) \Delta) \quad (6.25)$$

and the state equation is

$$\theta_t = I\theta_{t-1} \quad (6.26)$$

where I is an identity matrix. The CIF models the receptive field of the neuron as a Gaussian function:

$$\lambda(x_t, \theta_t) = \exp\left(\alpha_t - \frac{(x_t - \mu_t)^2}{2\sigma_t^2}\right) \quad (6.27)$$

and $\theta_t = (\alpha_t, \mu_t, \sigma_t^2)$.

The joint probability density of a neural spike train may be written as

$$p(y_{0:T}) = \exp\left\{\int_0^T \log \lambda(u|H_u) dy(u) - \int_0^T \lambda(u|H_u) du\right\} \quad (6.28)$$

If the probability density in Eq. (6.28) depends on estimation of an unknown q -dimensional parameter θ , then the logarithm of Eq. (6.28) viewed as a function of θ given $y_{0:T}$ is the sample path of the log likelihood defined as

$$L(\theta|y_{0:T}) = \int_0^T \ell_u(\theta) du \quad (6.29)$$

where $\ell_u(\theta)$ is the integrand in Eq. (6.29) or the “instantaneous” log likelihood defined as

$$\ell_t(\theta) dt = \log[\lambda(t|H_t, \theta)] y_t - \lambda(t|H_t, \theta). \quad (6.30)$$

Heuristically, Eq. (6.30) measures the instantaneous accrual of “information” from the spike train about the parameter θ . We use it as the criterion function in our point process adaptive filter algorithm.

To derive an adaptive point process filter algorithm we assume that the q -dimensional parameter θ in the instantaneous log likelihood, Eq. (6.30) is time-varying. The interval $(0, T]$ is divided into equal bins with bin width Δ . The parameter estimates are updated at every time bin indexed by t . A standard prescription for constructing an adaptive filter algorithm to estimate a time-varying parameter is to use the instantaneous steepest descent (Haykin, 2002):

$$\hat{\theta}_t = \hat{\theta}_{t-1} - \varepsilon \nabla \ell_t(\hat{\theta}_{t-1}) \quad (6.31)$$

which, by a rearrangement of terms, gives the *instantaneous steepest descent* adaptive filter algorithm for point process observations (Brown et al., 2001):

$$\hat{\theta}_t = \hat{\theta}_{t-1} - \varepsilon \nabla \log \lambda(t|H_t, \hat{\theta}_{t-1}) [y_t - \lambda(t|H_t, \hat{\theta}_{t-1}) \Delta]. \quad (6.32)$$

Namely, the parameter update $\hat{\theta}_t$ at t is the previous parameter estimate $\hat{\theta}_{t-1}$ plus a dynamic gain coefficient, $-\varepsilon \nabla \log \lambda(t|H_t, \hat{\theta}_{t-1})$, multiplied by an innovation or error signal $[y_t - \lambda(t|H_t, \hat{\theta}_{t-1}) \Delta]$. The error signal provides the new information coming from the spike train and is defined by comparing the predicted probability of a spike, $\lambda(t|\hat{\theta}_{t-1}) \Delta$, at t with y_t , which is 1 if a spike is observed in $((t-1), t]$ and 0 otherwise. How much the new information is weighted depends on the magnitude of the dynamic gain coefficient. The parallel between the error signal in Eq. (6.32) and that in standard recursive estimation algorithms suggests that the instantaneous log likelihood is a reasonable criterion function for adaptive filters with point process observations. The instantaneous steepest descent algorithm can also be derived as a special case of the point process filter by setting $W_{t|t-1} = \varepsilon$ at each update.

We used the instantaneous steepest descent algorithm to track the evolution of the place field from the neural spiking activity in the rat CA1 neuron shown in Figure 6.3. The activity was recorded for 1200 seconds of the animal running back and forth on the U-shaped track. The evolution of the individual parameters across the experiment is shown in Figure 6.4. During the 20 minutes of the experiment, the center of the place field moved from 85 cm to 65 cm, the scale of the field increased from 10 cm to 16 cm, and the amplitude of the field increased from 1 spike/sec to 27 spikes/sec. The evolution of the place field can be seen in Figure 6.5, which shows its shape at four different time points. The displacement of the field and its growth in height and scale are evident. The maximum likelihood estimate of the field (the dashed line in the figure), computed using a static model, overestimated the field's shape and location during the early part of the experiment, and underestimated them during the latter part of the experiment.

These results illustrate that even in an environment that is familiar to the animal the place receptive fields change their representations of the space. The instantaneous steepest descent algorithm allows us to track those changes on a millisecond-to-millisecond time scale.

6.3.3 Tracking Spatial Receptive Field and Particle Filtering

The challenge of using the Bayes-Chapman-Kolmogorov equations is in evaluating Eqs. (6.1) and (6.2) for a generic set of observation and state equations.

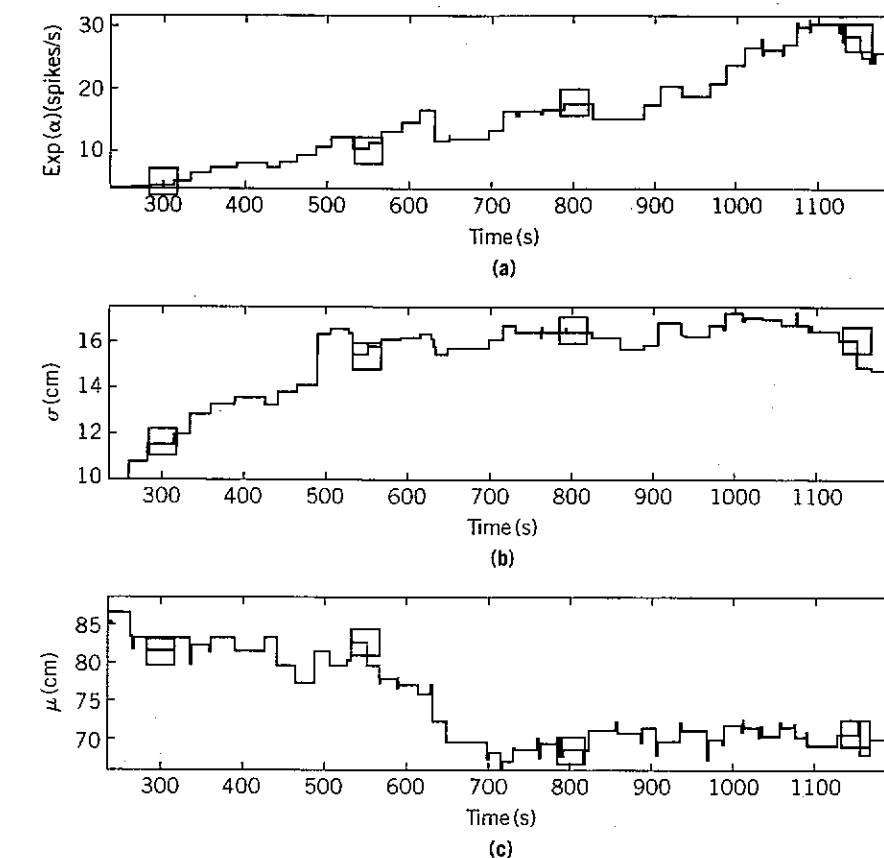


FIGURE 6.4

Adaptive filter estimates of the trajectories. (a) Maximum spike rate, $\exp(\alpha)$. (b) Place field scale, σ . (c) Place field center. Adaptive estimates were updated at 1-ms intervals. The squares in the panels at 300, 550, 800, and 1150 s are the times at which the place fields are displayed in Figure 6.5. The growth of the maximum spike rate (a), the variability of the place field scale (b), and the migration of the place field center (c) are all readily visible.
Source: Brown et al. (2001), *Proceedings of National Academy of Sciences*, Reprinted with permission, copyright © 2001 National Academy of Science, U.S.A.

As noted earlier, there are four computational approaches to performing Bayesian calculations: analytically, Gaussian or other approximation, exact numerical integration, and Monte Carlo. As an alternative to the point process filter algorithms, we can develop sequential Monte Carlo (SMC) or particle filter algorithms for evaluating the Bayes-Chapman-Kolmogorov system. The SMC algorithm is a recursive Monte Carlo procedure for simulating Eqs. (6.1) and (6.2). When the Monte Carlo samples or particles used in the algorithm

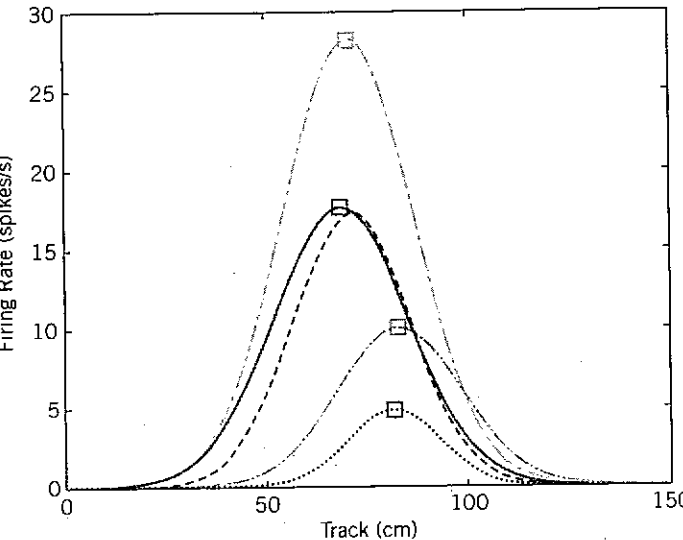


FIGURE 6.5

Estimated place fields at times 300 (dotted line), 550 (spike above dotted line), 800 (solid line), and 1150 (highest spike) sec. As in Figure 6.4, the black dashed line is the maximum likelihood estimate (MLE) of the place field obtained by using all the spikes in the experiment. The MLE ignores the temporal evolution of the place field. Please see this figure in color at the companion web site: www.elsevierdirect.com/companions/9780123750273

Source: Brown et al. (2001), *Proceedings of National Academy of Sciences*, Reprinted with permission, copyright © 2001 National Academy of Science, U.S.A.

are properly placed, weighted, and propagated, this system can be estimated sequentially through time. Moreover, it can be shown that as the number of particles increases, the output of the algorithm approaches an exact evaluation of these equations (Doucet et al., 2001; Cappé et al., 2005, 2007).

To define the SMC algorithm, we let π denote the proposal probability density, which defines the probability density from which we sample the particles at each time t of the algorithm, and we let $p(\theta_0)$ define the probability density for the state at time 0. We let $\hat{\theta}_t^{(i)}$ denote the value of particle i at t , and we let $w_t^{(i)}$ denote the weight of particle i at t for $i = 1, \dots, M$, where M is the total number of particles sampled at each update of the algorithm. The SMC algorithm is therefore given by

Step 1. Set $t = 0$ and, for $i = 1, \dots, M$ particles, draw the initial states $\theta_0^{(i)}$ from the $p(\theta_0)$ and set $w_0^{(i)} = M^{-1}$ for all i . Set $t = 1$.

Step 2. For $i = 1, \dots, M$, sample $\hat{\theta}_t^{(i)}$ from $\pi(\theta_t | \theta_{0:t-1}^{(i)}, y_{1:t})$ and set $\hat{\theta}_{0:t}^{(i)} = (\theta_{0:t-1}^{(i)}, \hat{\theta}_t^{(i)})$. Evaluate the importance weights:

$$w_t^{(i)} = w_{t-1}^{(i)} \frac{p(y_t | \hat{\theta}_t^{(i)}) p(\hat{\theta}_t^{(i)} | \theta_{0:t-1}^{(i)})}{\pi(\hat{\theta}_t^{(i)} | \theta_{0:t-1}^{(i)}, y_{1:t})}$$

Normalize the importance weights:

$$\tilde{w}_t^{(i)} = w_t^{(i)} \left[\sum_{j=1}^M w_t^{(j)} \right]^{-1}$$

Step 3. Resample with replacement M particles $\theta_{0:t}^{(i)}$; $i = 1, \dots, M$ from the set $(\hat{\theta}_{0:t}^{(i)}; i = 1, \dots, M)$ with selection probability defined by the normalized importance weights $(\tilde{w}_t^{(i)})$, and using the sampling-resampling method (SIR) with added jitter (Djuric, 2001), to obtain samples approximately distributed according to $p(\theta_{0:t}^{(i)} | y_{0:t})$. For $i = 1, \dots, M$, set $w_t^{(i)} = \tilde{w}_t^{(i)} = M^{-1}$ to obtain the Monte Carlo probability density

$$p(\theta_{0:t}^{(i)} | y_{1:t}) \approx M^{-1} \sum_{i=1}^M \delta_{\theta_{0:t}^{(i)}}(d\theta_{0:t})$$

where $\delta_{\theta_{0:t}^{(i)}}$ is the Dirac delta function indicating a point mass at $\theta_{0:t}^{(i)}$.

Step 4. Compute any summary statistics of interest as

$$E[g_t(\theta_{0:t})] = \int g_t(\theta_{0:t}) p(\theta_{0:t} | y_{1:t}) d\theta_{0:t} \approx M^{-1} \sum_{i=1}^M g_t(\theta_{0:t}^{(i)})$$

where, for example, $g(\theta) = \theta$ gives the estimate of the conditional mean $\mu_{t|t}$, and $g_t(\theta_t) = \theta_t \theta_t' - \mu_{t|t} \mu_{t|t}'$ gives the estimate of the conditional variance. Set $t = t + 1$. If $t \leq T$, return to step 2; otherwise stop.

The SMC methods have been successfully applied to the problem of movement decoding from neural spike activity recorded in motor cortex (Brockwell

et al., 2004; Shoham et al., 2005; Brockwell et al., 2007). In particular, they have been applied to the problem of tracking the two-dimensional spatial receptive field of a rat hippocampal neuron. The specific filter used in this analysis combines both SMC and point process filter (PPF) techniques, and has been referred to as the SMC-PPF algorithm (Ergun et al., 2007). Here the PPF algorithm is used to directly compute the proposal density.

We illustrate the algorithm as applied in an actual experiment by analyzing a spike train recorded from a single pyramidal neuron in the CA1 region of the rat hippocampus, recorded while the animal foraged for 900 s in a 70-cm-diameter open circular environment. As illustrated in Section 6.3.2 hippocampal neurons have well-defined spatial receptive fields with known dynamic properties, particularly in one-dimensional linear environments. Because the dynamics of these receptive fields have been less well studied in two-dimensional environments, we used the SMC-PPF algorithm to analyze the temporal evolution of a hippocampal neuron's receptive field. We model the two-dimensional spatial receptive field as an exponentiated, linear combination of Zernike polynomials and rewrite Eq. (6.8) as

$$\lambda(t|x_t, \theta_t) = \exp \left\{ \sum_{\ell=0}^L \sum_{m=-\ell}^{\ell} \theta_t^{\ell, m} z_\ell^m(x_t) \right\} \quad (6.33)$$

where z_ℓ^m is the m^{th} component of the ℓ^{th} -order Zernike polynomial, $\theta_t^{\ell, m}$ is the associated coefficient, and $x_t = [x_{1,t}, x_{2,t}]$ is the position of the animal at time t . The Zernike polynomials form an orthogonal basis whose support is restricted to the circular environment. Following Barbieri et al. (2004), the trade-off between model flexibility and computational complexity is balanced by choosing $L = 3$, yielding a total of 16 coefficients of which 10 are nonzero. The CIF defines the spatial receptive field of the neuron. In order to track the temporal evolution of the receptive field, it suffices to track the temporal evolution of $\theta_t = [\theta_t^{0,0} \ \theta_t^{1,-1} \ \dots \ \theta_t^{3,3}]$, which is the vector of the 10 nonzero Zernike coefficients. It is assumed that the state space model for the Zernike coefficients is a Gaussian random-walk model:

$$\theta_t = \theta_{t-1} + \eta_t \quad (6.34)$$

with zero mean and variance Σ_η . In this analysis, a total of 10,000 particles was used, and the Zernike coefficients were updated at $\Delta = 33$ ms. Initial $Q = I_{10 \times 10} \sigma^2$ was chosen as the diagonal covariance matrix, where $\sigma^2 = 1 \times 10^{-3}$, and θ_0 , the maximum likelihood estimate of the parameter computed for this

6.3 Applications of the State Space Paradigm in Neuroscience

neuron from the preceding 500 s in this experiment, was used as the initial guess of the Zernike coefficients.

The results from this analysis are presented in Figure 6.6. To display all the position and spike train data, the experimental data are subdivided into nine consecutive 100-s epochs (parts (a) through (i) of the figure). In each panel, the upper plot shows the trajectory of the animal during the 100-s interval, with the spiking activity of the neuron superimposed as light gray asterisks on the trajectory to show the location of the animal at the time each spike was fired. The lower plot in each panel shows the intensity function computed by averaging the means of the estimated SMC-PPF posterior densities for each of the 10 Zernike coefficients in that 100-s segment. The spiking activity was concentrated initially in the upper left area of the environment

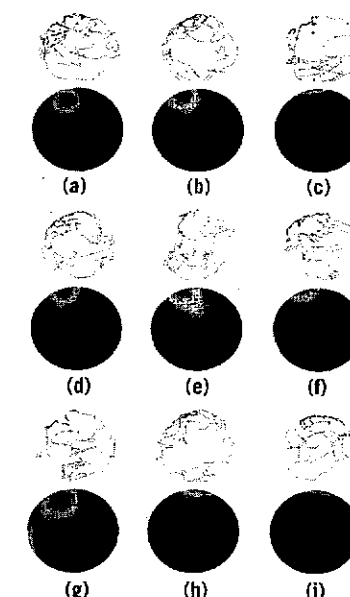


FIGURE 6.6

Tracking the temporal evolution of a 2D place field. Results are presented subdividing the 900-s experiment into nine consecutive 100 s of exploration in a circular environment 70 cm in diameter (from (a) to (i)). For each subplot, the upper panel shows the trajectory of the animal (dark gray curves) during the 100-s interval, with the spiking activity of the neuron superimposed on the trajectory (light gray asterisks). The lower panel of each subplot shows the 2D spatial receptive field computed from the average of the ten Zernike coefficients estimated in each 100-s segment. Please see this figure in color at the companion web site: www.elsevierdirect.com/companions/9780123750273

Source: Ergun et al. (2007), *IEEE Transactions on Biomedical Engineering*, Reprinted with permission, copyright © 2007 IEEE.

(Figure 6.6(a)–(b), upper panel) and the shape of the receptive field was more symmetric, with its higher-intensity peak located in the upper left area (Figure 6.6(a)–(b), lower panel).

Between 201 and 300 s, the spiking activity concentrated around the upper rim of the environment (Figure 6.6(c), upper panel); between 301 to 400 s, it reemerged in the upper left area (Figure 6.6(d), upper panel); then, between 401 to 500 s, it spread into the center of the environment (Figure 6.6(e), upper panel). From 501 to 600 s, the spiking activity was once again concentrated on the upper rim of the environment (Figure 6.6(f), upper panel). The change in the location of the spiking activity is captured nicely by the dynamic of the receptive fields between 201 and 600 s estimated from the SMC-PPF (Figure 6.6(c)–(f), lower panels). The spiking activity showed a similar pattern from 601 to 700 s (Figure 6.6(g)–(i), upper panels), and the SMC-PPF estimates of the receptive fields (Figure 6.6(g)–(i), lower panels) once again tracked this evolution. During the 900-s recording session of this experiment, the center of this spatial receptive field migrated 50 cm.

These results show that the SMC-PPF algorithm tracked the dynamics of this neuron's spatial receptive field; they also illustrate that the temporal evolution of the spatial receptive fields of hippocampal pyramidal neurons observed in linear environments can be observed in open circular environments as well.

6.3.4 Dynamic Analysis of Behavioral Learning Experiments and the Expectation-Maximization Algorithm

Learning experiments in neuroscience can be analyzed using a state space model with a discrete observation process. A learning experiment consists of a sequence of trials in which a subject executes a task correctly or incorrectly. That is, we have a sequence of learning trials with binary responses and we let y_t denote the response in trial t , where $y_t = 1$ is a correct response (Figure 6.7, medium gray dots at top of the panel) and $y_t = 0$ is an incorrect response (Figure 6.7, dark gray dots at the top of the panel).

We let p_t denote the probability of a correct response t . At trial t , the observation model defines the probability of observing y_t given the value of the cognitive state process x_t . The observation model is the Bernoulli probability mass function:

$$\Pr(y_t|p_t, x_t) = p_t^{y_t} (1 - p_t)^{1-y_t} \quad (6.35)$$

where p_t is defined by the logistic equation

$$p_t = [1 + \exp(\mu + x_t)]^{-1} \exp(\mu + x_t) \quad (6.36)$$

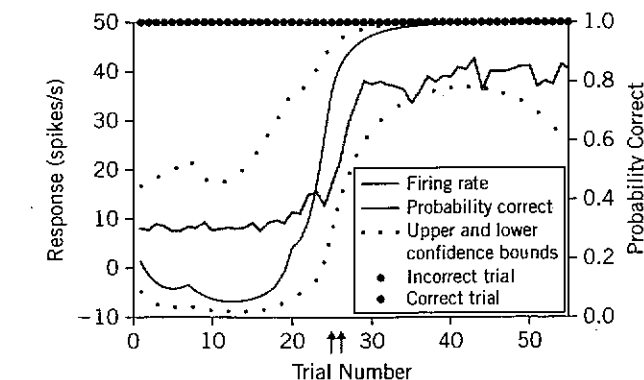


FIGURE 6.7

Sequence of correct responses (dark gray dots) and incorrect responses (medium gray dots) from a monkey executing a location-scene association task. Learning curve (solid dark gray curve) and 90% confidence intervals (dark gray dotted curves) are shown. The medium gray curve is the estimated firing rate of a hippocampal neuron recorded simultaneously as the animal executed the task. The dark gray horizontal line is the probability of a correct response by chance. Please see this figure in color at the companion web site: www.elsevierdirect.com/companions/9780123750273

Source: Wirth et al. (2003), *Science*, Reprinted with permission, Copyright © 2003 AAAS.

and μ is determined by the probability of a correct response by chance in the absence of learning or experience. We define the unobservable cognitive state process as a random walk:

$$x_t = x_{t-1} + \varepsilon_t \quad (6.37)$$

where the ε_t are independent Gaussian random variables with mean 0 and variance σ_ε^2 . In this analysis the objective is to estimate the learning curve—that is, the probability of a correct response as a function of trial number given the entire sequence of correct and incorrect responses in the experiment. Unlike the other examples we have discussed, this is a state space smoothing problem. In other words, we wish to estimate the most likely values of the learning curve at each time given all of the data in the experiment.

In the learning example, we let $x = x_{1:T}$ be the vector of the unobservable or hidden cognitive state process; x_0 and σ_ε^2 are parameters. We use the expectation-maximization (EM) algorithm to estimate them by maximum likelihood (Dempster et al., 1977). The EM algorithm is a well-known procedure for performing maximum likelihood estimation when there is an unobservable process or missing observations. We used it to estimate state space models from point process observations with linear Gaussian state

processes (Smith and Brown, 2003). The current EM algorithm is a special case of the same algorithm in Smith and Brown (2003).

We state first the general formulation of the EM algorithm. If y is the observed data, x is the missing or unobservable data, and θ is the parameter to be estimated, then the EM algorithm maximizes the likelihood $p(y|\theta)$ by iterating between an expectation step (E-step) and a Maximization step (M-step). To do so, we define the complete data likelihood $p(y,x|\theta)$. The general formulation is as follows. Given an estimate of the parameter θ at iteration ℓ we compute the in step $\ell+1$ as follows:

$$\text{E-step: } Q(\theta|\theta^{(\ell)}) = E[\log p(y,x|\theta)||y,\theta^{(\ell)}] \quad (6.38)$$

which is the expectation of the complete data log likelihood.

$$\text{M-step: } \theta^{(\ell+1)} = \max_{\theta} Q(\theta|\theta^{(\ell)}). \quad (6.39)$$

The algorithm iterates between the E-step in Eq. (6.38) and the M-step in Eq. (6.39). The maximum likelihood estimate of θ is $\theta_{ML} = \lim \theta^{(\ell)}_{\ell \rightarrow \infty} = \theta^{(\infty)}$.

The use of the EM algorithm to analyze our state space learning model here requires computing the complete data likelihood, which is the joint probability density of $y_{1:T}$ and x . The EM algorithm allows computing the maximum likelihood estimate of x_0 and σ_e^2 and hence, the learning curve. The complete data likelihood is

$$\begin{aligned} p(y_{1:T},x|\sigma_e^2, x_0) &= \prod_{t=1}^T p_t^{y_t} (1-p_t)^{1-y_t} p(x|\sigma_e^2, x_0) \\ &= p(y_{1:T}|x)p(x|\sigma_e^2, x_0) \end{aligned} \quad (6.40)$$

where the first term on the right-hand side is defined by the Bernoulli probability mass function in Eq. (6.35), and second term is the joint probability density of the cognitive state process defined by the Gaussian model in Eq. (6.37). At iteration $(\ell+1)$ of the algorithm, we compute in the E-step the expectation of the complete data log likelihood given the responses $y_{1:T}$ across the T trials and $\sigma_e^{2(\ell)}$, as well as the parameter estimate from iteration ℓ , which is defined as follows:

6.3 Applications of the State Space Paradigm in Neuroscience

E-Step:

$$\begin{aligned} Q(\sigma_e^2|\sigma_e^{2(\ell)}) &= E\left[\log p(y_{1:T},x|\sigma_e^2)\middle|y_{1:T},\sigma_e^{2(\ell)},x_0\right] \\ &= E\left[\sum_{t=1}^T n_t(\mu + x_t) - \log[1 + \exp(\mu + x_t)]\middle|y_{1:T},\sigma_e^{2(\ell)},x_0\right] \\ &\quad + E\left[\sum_{t=1}^T -\frac{1}{2} \frac{(x_t - x_{t-1})^2}{\sigma_e^2} - \frac{T}{2} \log 2\pi - \frac{T}{2} \log \sigma_e^2\middle|y_{1:T},\sigma_e^{2(\ell)},x_0\right] \end{aligned} \quad (6.41)$$

Expanding the right-hand side of Eq. (6.41), we see that calculating the expected value of the complete data log likelihood requires computing the expected value of the state variable $E[x_t||y_{1:T},\sigma_e^{2(\ell)},x_0]$, and the covariances $E[x_t^2||y_{1:T},\sigma_e^{2(\ell)},x_0]$ and $E[x_t x_{t+1}||y_{1:T},\sigma_e^{2(\ell)},x_0]$. We denote them as

$$x_{t|T} \equiv E[x_t||y_{1:T},\sigma_e^{2(\ell)},x_0] \quad (6.42)$$

$$W_{t|T} \equiv E[x_t^2||y_{1:T},\sigma_e^{2(\ell)},x_0] \quad (6.43)$$

$$W_{t,t+1|T} \equiv E[x_t x_{t+1}||y_{1:T},\sigma_e^{2(\ell)},x_0] \quad (6.44)$$

for $t = 1, \dots, T$. To compute these quantities efficiently we decompose the E-step into three parts: a nonlinear recursive filter algorithm to compute $x_{t|t}$, a fixed-interval smoothing algorithm to estimate $x_{t|T}$, and a state space covariance algorithm to estimate $W_{t|T}$ and $W_{t,t-1|T}$. The specific algorithms for our model are

Filter Algorithm. Given $\sigma_e^{2(\ell)}$, we first compute recursively the state variable, $x_{t|t}$, and its variance, $\sigma_{t|t}^2$. We accomplish this using the filter algorithm (Smith and Brown, 2003):

- One-step prediction:

$$x_{t|t-1} = x_{t-1|t-1} \quad (6.45)$$

- One-step prediction variance:

$$\sigma_{t|t-1}^2 = \sigma_{t-1|t-1}^2 + \sigma_e^{2(\ell)} \quad (6.46)$$

- Posterior mode:

$$x_{t|t} = x_{t|t-1} + \sigma_{t|t-1}^2 [y_t - p_{t|t}] \quad (6.47)$$

- Posterior variance:

$$\sigma_{t|t}^2 = \left[(\sigma_{t|t-1}^2)^{-1} + p_{t|t}(1 - p_{t|t}) \right]^{-1} \quad (6.48)$$

where $p_{t|t}$ is computed from Eq. (6.36) evaluated at $x_{t|t}$ for $t = 1, \dots, T$ and $j = t$. The initial condition is $x_0 = 0$ and $\sigma_{0|0}^2 = \sigma_\varepsilon^{2(\ell)}$. The algorithm is nonlinear because $x_{t|t}$ appears on both left- and right-hand sides of Eq. (6.47). The derivation of this algorithm for the arbitrary point process observation model and the linear state space model is given in Smith and Brown (2003).

Fixed-Interval Smoothing Algorithm. Given the sequence of posterior mode estimates $x_{t|t}$ (Eq. (6.47)) and the variance $\sigma_{t|t}^2$ (Eq. (6.48)), we use the fixed-interval smoothing algorithm (Shumway and Stoffer, 1982; Mendel, 1995; Brown et al., 1998; Smith and Brown, 2003) to compute $x_{t|T}$ and $\sigma_{t|T}^2$. The smoothing algorithm is formulated as

$$x_{t|T} = x_{t|t} + A_t(x_{t+1|T} - x_{t+1|t}) \quad (6.49)$$

$$A_t = \sigma_{t|t}^2 (\sigma_{t+1|t}^2)^{-1}$$

$$\sigma_{t|T}^2 = \sigma_{t|t}^2 + A_t^2 (\sigma_{t+1|T}^2 - \sigma_{t+1|t}^2) \quad (6.50)$$

for $t = T-1, \dots, 1$ and initial conditions $x_{T|T}$ and $\sigma_{T|T}^2$.

State Space Covariance Algorithm. The covariance estimate, $\sigma_{t,u|T}$, can be computed from the state space covariance algorithm (de Jong and MacKinnon, 1988) and is given as

$$\sigma_{t,u|T} = A_t \sigma_{t+1,u|T} \quad (6.51)$$

for $1 \leq t \leq u \leq T$.

It follows that the expectations required in Eq. (6.42) are given by Eq. (6.49) and that the covariance terms required for Eqs. (6.43) and (6.44) of the E-step in the EM algorithm are

$$W_{t,t-1|T} = \sigma_{t-1,t|T} + x_{t|T} x_{t-1|T} \quad (6.52)$$

and

$$W_{t|T} = \sigma_{t|T}^2 + x_{t|T}^2. \quad (6.53)$$

In the M-step we maximize the expected value of the complete data log likelihood in Eq. (6.41) with respect to $\sigma_\varepsilon^{2(\ell+1)}$, which yields

$$\text{M-Step: } \sigma_\varepsilon^{2(\ell+1)} = T^{-1} \left(2 \left(\sum_{t=1}^T W_{t|T} - \sum_{t=1}^T W_{t-1,t|T} \right) - (W_{T|T} - W_{0|T}) \right). \quad (6.54)$$

The algorithm iterates between the E-step (Eq. (6.41)) and the M-step (Eq. (6.54)). The maximum likelihood estimate of σ_ε^2 is $\sigma_\varepsilon^{2(\infty)}$. The convergence criteria for the algorithm are those used in Smith and Brown (2003). The filter algorithm (Eqs. (6.45) through (6.48)), evaluated at the maximum likelihood estimate of σ_ε^2 , together with Eq. (6.36), give the filter algorithm estimate of the learning curve, whereas the fixed-interval smoothing algorithm evaluated at a maximum likelihood estimate of σ_ε^2 (Eqs. (6.49) through (6.50)), together with Eq. (6.36), give the maximum likelihood (empirical Bayes) or smoothing algorithm estimate of the learning curve (Smith et al., 2004).

We illustrate the algorithm applied to an actual learning experiment by analyzing the sequence of correct and incorrect responses of a macaque monkey in a location-scene association task, described in detail in Wirth et al. (2003). In this task, each trial started when the monkey fixated on a centrally presented cue on a computer screen. The animal was then presented with four identical targets (north, south, east, and west) superimposed on a novel visual scene. After the scene disappeared, the targets remained on the screen during a delay period. At the end of the delay period, the fixation point disappeared, cueing the animal to make an eye movement to one of the four targets. For each scene, only one target was rewarded and the positions of rewarded locations were counterbalanced across all new scenes. Two to three novel scenes were typically learned simultaneously, and trials of novel scenes were interspersed with trials in which two to four well-learned scenes were presented. Because there were four locations, the monkey could choose as a response; the probability of a correct response occurring by chance was 0.25. To characterize learning, the correct and incorrect responses as a function of trial number were recorded for each scene (Figure 6.7). The objective of the study was to track learning as a function of trial number and to relate it to changes in the activity of simultaneously recorded hippocampal neurons (Wirth et al., 2003).

Figure 6.7 shows the correct responses (medium gray dots) and incorrect responses (dark gray dots) responses given by the monkey across 55 trials for one novel scene. The sequence of correct and incorrect responses and the

learning curve (Figure 6.7, dark gray curve) show that the animal's performance changed dramatically after approximately trial 23. The 90% confidence intervals for the learning curve were computed using the change-of-variable formula in Smith et al. (2004). With the criterion of the trial being that beyond which performance better than chance was certain with a probability of at least 0.95 for the balance of the experiment (Smith et al., 2004), the learning trial was identified as trial 23 (Figure 6.7, dark gray arrow). A dynamic estimate of the spike rate function (Figure 6.7, medium gray curve) for a hippocampal neuron was computed using the instantaneous steepest descent algorithm (Eq.(6.32)). The trial in which the spiking activity of the neurons was identified as being different from baseline was trial 24 (Figure 6.7, medium gray arrow). The change in the spike rate function for this neuron occurred almost simultaneously with the change in the monkey's performance of the task, which suggests that the neuron's activity mirrored the learning process.

These results illustrate how the state space smoothing algorithm for binary responses can be used along with the instantaneous steepest descent algorithm to relate changes in behavior on a learning task to changes in the activity of hippocampal neurons.

6.3.5 Markov Chain Monte Carlo Methods and the Analysis of Cortical UP/DOWN States

Neuronal UP and DOWN states, the periodic fluctuations between increased and decreased spiking activity of a neuronal population, are fundamental features of cortical circuits (Battaglia et al., 2004; Haider et al, 2007; Ji and Wilson, 2007). Developing quantitative descriptions of UP/DOWN state dynamics is important for understanding how these circuits represent and transmit information. Given multiunit spike train recordings, the objective of the analysis is to estimate the states, the location, and the number of state transitions, and parameters associated with the sojourn time probability densities of the states. This is a joint state and parameter estimation problem, in which the state is discrete and the parameter is static. For this purpose, we develop an EM algorithm.

The E-step of the EM algorithm requires computing the distribution of the missing data or hidden states conditional on the observed data and the current parameter estimate (Eq. (6.38)). In the applications of this algorithm presented earlier, we used Gaussian approximations to compute these conditional distributions. In recent years many new techniques have been developed in Bayesian analyses to compute conditional or posterior distributions. Therefore, in principle, any Bayesian method used to compute posterior distributions may be used to evaluate the conditional distributions in the E-step

of an EM algorithm. Markov chain Monte Carlo method (MCMC) techniques are now among those principally used to conduct Bayesian analyses (Spall, 2003; Gelman et al., 2004; Robert and Casella, 2004). In our analysis of cortical UP/DOWN states, we use the MCMC method to evaluate the conditional distributions in the E-step because it provides an efficient way to determine a critical unknown in this problem: the number of transitions between the UP and DOWN states. These algorithms are termed MCEM algorithms (Chan and Ledolter, 1995; Tanner, 1996; McLachlan and Krishnan, 2008).

When posterior distributions cannot be computed exactly, numerical methods are not feasible because an analytic approximation may be inaccurate. MCMC methods can often be constructed to simulate posterior distributions by appropriately structured random sampling. Instead of drawing independent samples from the posterior distribution directly, the MCMC algorithm constructs a Markov chain of sample draws whose equilibrium distribution comes near to the posterior distribution desired. That is, sample $i + 1$ is drawn conditional on sample i following a Markov chain rule. The key step in designing an MCMC algorithm is the choice of proposal density that governs the transition between sample draws. The Markov chain theory states that, given an arbitrary initial value, the chain will converge to the equilibrium point provided that the chain is run for a sufficiently long period of time. Various statistical tests have been developed to assess convergence (Brooks and Gelman, 1998; Gelman et al., 2004).

In most applications of MCMC algorithms, the dimension of the posterior distribution to be estimated is fixed. However, there are problems for which the dimension of the posterior distribution is unknown and must be determined as part of the analysis. The study of cortical UP/DOWN states presents such challenges because the unknown dimension is indeed the number of state transitions. For this purpose, we use reversible jump MCMC (RJMCMC), for which the proposal density generates moves reversibly among parameter spaces of different dimensions (Green, 1995). Analysis with an RJMCMC method yields estimates of the states and a probability density over the dimension of the states.

To formulate the RJMCMC, we consider the transition from a current state space X to another state space X' , where $\dim(X) \neq \dim(X')$. Let $R^{(i)}(X \rightarrow X'|\theta)$ be the proposal density associated with the proposal X' for the move type i , and let q_i be the probability of choosing the move type (i) . The proposal density for the move from a current state X to X' is thus given by

$$R(X \rightarrow X'|\theta) = \sum_i q_i R^{(i)}(X \rightarrow X'|\theta). \quad (6.55)$$

The acceptance probability for the move $X \rightarrow X'$ is given by $A = \min\{1, B\}$, where

$$B = \frac{p(y, X'|\theta)R(X' \rightarrow X|\theta)}{p(y, X|\theta)R(X \rightarrow X'|\theta)}|J| = \frac{p(y|X', \theta)p(X'|\theta)R(X' \rightarrow X|\theta)}{p(y|X, \theta)p(X|\theta)R(X \rightarrow X'|\theta)}|J|. \quad (6.56)$$

$p(y, X|\theta)$ is an unnormalized posterior density or, in our case, a complete data likelihood, and $|J|$ is the determinant of the Jacobian of a mapping from X to X' . If there is no change in dimension, then $|J| = 1$.

For the current UP/DOWN estimation problem, we model the state as binary (0–1) being either DOWN or UP, and we assume that a Markov or semi-Markov model governs the transitions between the states. To estimate the UP/DOWN states from multiunit spiking activity, we develop a continuous-time Markov discrete state space model with time-varying state transition with point process observations. Let X_t be the state of the continuous-time Markov process at time t , which is 0 for the DOWN state and 1 for the UP state. Let $\xi_k(j, i) = \Pr(X_{k-1} = j, X_k = i)$ be the transition probability from state j to state i at the k^{th} sojourn, $F(t|\theta_j)$ be the cumulative distribution function of the sojourn time for the DOWN states for $j = 0$ and for the UP states for $j = 1$. We let τ_k be the length of the k^{th} sojourn time, $v_k = \sum_{i=0}^{k-1} \tau_i$ for $k = 1, \dots, n$, where n is the total number of state jumps or transitions. We model the sojourn time distributions for the UP and DOWN states, respectively, as exponential and log normal. It is assumed that, conditional on the state X_t , the recorded C tetrodes of multiunit spiking activity are conditionally independent. We model the CIF for the multiunit activity on tetrode c for $c = 1, \dots, C$ by a generalized linear model:

$$\log \lambda(t|\theta^c, X_t) = \mu^c + \alpha^c X_t + \int_0^t \exp(-\beta^c(t-u))dy(u) \quad (6.57)$$

where $\theta^c = (\mu^c, \alpha^c, \beta^c)$. The complete data likelihood function is

$$\begin{aligned} p(y, X_{0:T}|\theta) &= p(y|X_{0:T}, \theta)p(X_{0:T}|\theta) \\ &= \exp\left(\sum_{c=1}^C \sum_{k=1}^n \int_{v_{k-1}}^{v_k} [\log \lambda^c(t|X_t, \theta^c) dy_t^c - \lambda^c(t|X_t, \theta^c) dt]\right) \\ &\times \prod_{i,j} [1 - F(\tau_k|\theta_j)]^{I_k(j,j)} [F(\tau_k|\theta_j)]^{I_k(j,i)} \end{aligned} \quad (6.58)$$

6.3 Applications of the State Space Paradigm in Neuroscience

205

where the first term on the right-hand side of Eq. (6.58) defines the multiunit activity conditional on the states, and the second term defines the probability of state transitions between the neighboring sojourns in which $I_k(j, i)$ is the indicator function for the transition from state j to state i at the k^{th} sojourn.

To illustrate this method, the above model was applied to the analysis of multiunit spiking recorded on $C = 8$ tetrodes in the primary somatosensory cortex of a rat. A single time series of approximately 15.7 minutes of multiunit spiking activity from the 8 tetrodes was constructed by concatenating multiunit activity recorded from 11 slow-wave sleep (SWS) periods with an average length of 85.7 s and with a standard deviation of 35.8 s. An MCEM algorithm using RJMCMC with seven categories of moves at each E-step was implemented to estimate the state transitions, to estimate $\xi_k(j, i)$ and to estimate n . The parameter θ was computed at the M-step. The details of this EM algorithm are given in Chen et al. (2009).

A 5-second segment of the data is shown in Figure 6.8. In the analysis we compared the MCEM method with a simpler hidden Markov model (HMM) also fit with an EM algorithm and an empirical, threshold-based method (Ji and Wilson, 2007). In the 5-second segment the state transitions identified by the HMM (Figure 6.8(b)) agreed most of the time with those identified by the threshold method (Figure 6.8(a)). In general, the MCEM method estimated less frequent state transitions than did the other two (Figure 6.8(c)) because the frame occurrence rates for the threshold, HMM and MCEM methods were respectively 95, 103, and 82 min⁻¹. The MCEM analysis gave fewer short sojourns because it allowed merges of neighboring sojourns during the RJMCMC procedure. The frame rate from our MCEM analysis was still greater than the rate of 43.5 min⁻¹ reported in the visual cortex recordings (Ji and Wilson, 2007).

These results show that it is possible to develop stochastic models and model fitting algorithms to analyze cortical UP/DOWN states, and that different model formulations can reach different conclusions regarding the number of state transitions. As more experimental evidence accrues on the properties of cortical UP/DOWN states, the future challenge will be to determine which model most accurately describes the underlying neurophysiology.

6.3.6 State Space Smoothing, Dynamic Parameter Estimation, and Analysis of Population Learning

In population learning studies, across-subject response differences are an important source of variance that must be characterized to accurately identify features of the learning process that are common to the population. Although

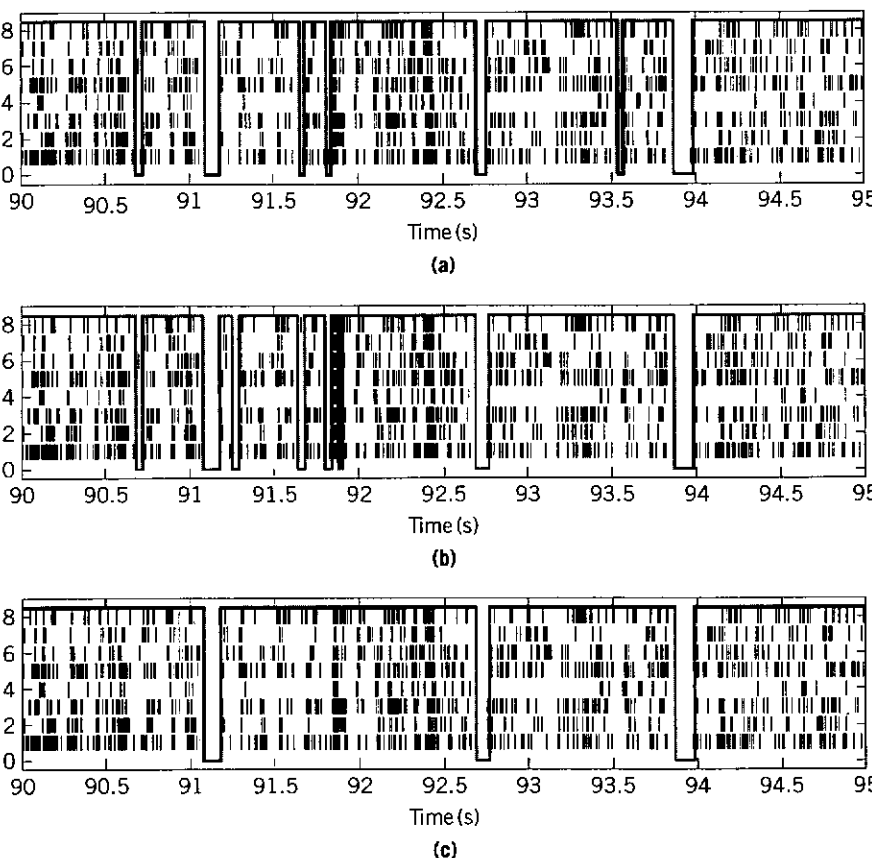


FIGURE 6.8

Multi-unit activity spike trains of 8 tetrodes recorded from the primary somatosensory cortex of one rat. (a) A selected 5-s segment of the MUA spike trains during SWS and its UP/DOWN state classification via the threshold-based method (segmented by the thick solid line). (b) The hidden state estimation result obtained from the discrete-time HMM (used as the initial state for the continuous-time RJMCMC sampler). (c) The hidden state estimation obtained from the MCEM algorithm. In this example, the MCEM algorithm merged several neighboring sojourns that were estimated differently from the HMM. Source: Chen et al. (2009), *Neural Computation*, reprinted with permission, Copyright © 2009 MIT Press.

learning is a dynamic process, current population analyses do not use dynamic estimation methods, nor do they compute both population and individual learning curves; rather, they use learning criteria that are less than optimal. We present a *state space random effects* (SSRE) model to estimate population and individual learning curves, ideal observer curves, and learning trials, and to

make dynamic assessments of learning between two populations and within the same population that avoid multiple hypothesis tests.

To define the model, we assume that J subjects participate in a learning experiment with T trials, where we index the trials by t for $t = 1, \dots, T$ and the subjects by j for $j = 1, \dots, J$. To define the observation equation we let y_j^k denote the response in trial t , from subject j , where $y_t^j = 1$ is a correct response and $y_t^j = 0$ is an incorrect response. We let p_t^j denote the probability of a correct response t from subject j . We assume that the probability of a correct response in trial t from subject j is governed by an unobservable learning state process x_t , which characterizes the dynamics of learning as a function of trial number. At trial t , for subject j , the observation model defines the probability of observing y_t^j , (i.e., either a correct or an incorrect response) given the value of the state process x_t . The observation model can be expressed as the Bernoulli probability mass function

$$Pr(y_t^j | p_t^j, x_t) = (p_t^j)^{y_t^j} (1 - p_t^j)^{1-y_t^j} \quad (6.59)$$

where p_t^j is defined by the logistic function

$$p_t^j = \exp(\mu + \beta^j x_t) [1 + \exp(\mu + \beta^j x_t)]^{-1}. \quad (6.60)$$

The parameter μ in Eq. (6.60) is determined by the probability of a correct response by chance in the absence of learning or experience, and β^j is the learning modulation parameter for subject j . We define the random effects component of our state space model by assuming that the modulation parameters β^j are independent Gaussian random variables with mean β_0 and variance $\sigma_\beta^2 I_{J \times J}$, where $I_{J \times J}$ is a $J \times J$ identity matrix. Therefore, we define the probability of a correct response for the population as

$$p_t = [1 + \exp(\mu + \beta_0 x_t)]^{-1} \exp(\mu + \beta_0 x_t). \quad (6.61)$$

We define the unobservable learning state process as a random walk:

$$x_t = x_{t-1} + \varepsilon_t \quad (6.62)$$

where the ε_t are independent Gaussian random variables with mean 0 and variance σ_ε^2 .

We construct a nonlinear recursive filtering algorithm, a fixed-interval smoothing algorithm, and a covariance smoothing algorithm to evaluate these expectations, as in Smith and Brown (2003) and Smith et al. (2004). To do so, we first construct the augmented state space model (Jones, 1993) in order

to include the random effects component of the model in the state equation. The augmented state space model is

$$\beta_t^* = \beta_{t-1}^* + \varepsilon_t^* \quad (6.63)$$

where $\beta_t^* = (x_t, \beta_t^1, \beta_t^2, \beta_t^3, \dots, \beta_t^J)$ and $\varepsilon_t^* = (\varepsilon_t, 0, \dots, 0)$. The stochastic properties of x_t are defined by Eq. (6.63), whereas the stochastic properties of β come from the assumption that the modulation parameters are jointly Gaussian-distributed with mean β_0 and covariance $\sigma_\beta^2 I_{J \times J}$. Our representation of the random effects in the state space model ensures that the stochastic properties of these parameters remain constant as the filter and smoothing algorithms evolve across trials (Jones, 1993). In summary, the algorithms are structured as follows.

Filter Algorithm. Given $\theta^{(\ell)}$, we can first compute recursively the state variable, $\beta_{t|t}^*$, and its variance, $W_{t|t}$. This is accomplished by using the following vector-valued nonlinear filter algorithm for the augmented state space model (Eden et al., 2004):

$$\beta_{t|t-1}^* = \beta_{t-1|t-1}^* \quad (6.64)$$

$$W_{t|t-1} = W_{t-1|t-1} + W_{\beta^*} \quad (6.65)$$

$$\beta_{t|t}^* = \beta_{t|t-1}^* + W_{t|t-1} F_t \quad (6.66)$$

$$W_{t|t} = [W_{t|t-1}^{-1} - G_t]^{-1} \quad (6.67)$$

$t = 1, \dots, T$, where W_{β^*} is the $(J+1) \times (J+1)$ diagonal covariance matrix whose $\{1,1\}$ element is $\sigma_\varepsilon^{2(\ell)}$ and whose remaining elements are 0, and where F_t is the $(J+1) \times 1$ vector whose elements are

$$F_t = \begin{bmatrix} \sum_{j=1}^J \beta_t^j (y_t^j - p_t^j) \\ x_t (y_t^1 - p_t^1) \\ \vdots \\ x_t (y_t^J - p_t^J) \end{bmatrix} \quad (6.68)$$

6.3 Applications of the State Space Paradigm in Neuroscience

and G_t is the $(J+1) \times (J+1)$ matrix whose elements are

$$G_{t,i,m} = \begin{cases} -\sum_{j=1}^J (\beta_t^j)^2 p_t^j (1-p_t^j) & i = m = 1 \\ -x_t \beta_t^i p_t^j (1-p_t^j) + (y_t^j - p_t^j) & i = 1, m = 2, \dots, J+1; \\ & i = 2, \dots, J+1, m = 1 \\ -x_t^2 p_t^j (1-p_t^j) & i = m = 2, \dots, J \\ 0 & \text{otherwise.} \end{cases} \quad (6.69)$$

The initial conditions are $\beta_0^{*(\ell)} = (x_0^{(\ell)}, \beta_0^{(\ell)})$ and

$$W_0 = \begin{bmatrix} \sigma_\varepsilon^{2(\ell)} & 0 \\ 0 & \sigma_\beta^{2(\ell)} I_{J \times J} \end{bmatrix}. \quad (6.70)$$

In these analyses we take $x_0^{(\ell)} = 0$.

The parameters are estimated using an EM algorithm as described in Section 6.3.4. The details of the algorithm are given in Smith et al. (2005).

To illustrate an application of the methods just described, we analyzed the learning behavior of four groups of rats in a set-shift experiment (Figure 6.9). Each animal executed 80 trials of a binary choice task. One group was treated with MK801 (treatment group), an NMDA antagonist used as a pharmacological model for schizophrenia; the other group received a placebo consisting of only the vehicle (vehicle group) in which the MK801 was dissolved. The animals in each group were further subdivided based on whether the reward arm on the previous day had been light or dark. The trial responses of the four groups are shown in Figure 6.9 as dark gray and light gray marks corresponding, respectively, to correct and incorrect responses across the 80 trials. In Figure 6.9, parts (a) and (b) (Figure 6.9, parts (c) and (d)) are the responses from the vehicle (treatment) group. Figure 6.9(a) (6.9(c)) shows the vehicle (treatment) animals rewarded for the light reward arm on the previous day, and Figure 6.9(b) (6.9(d)) shows the vehicle (treatment) animals rewarded for the dark reward arm on the previous day. Further subgroups were defined as vehicle light (6 animals), vehicle dark (7 animals), treatment light (3), and treatment dark (6).

Learning trials were identified using the criterion in Smith et al. (2004). The objective of the analysis was to estimate, for each animal, the individual

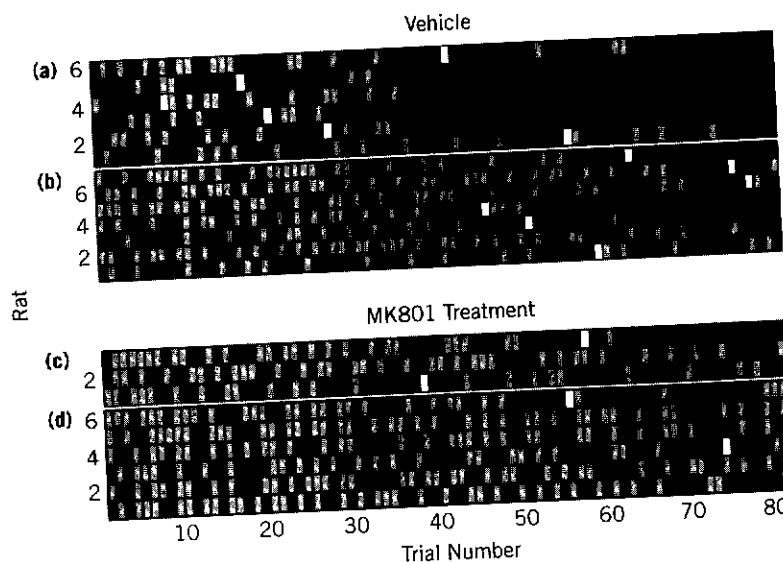


FIGURE 6.9

Behavior learning with multiple subjects. Responses of the 13 rats in the vehicle group ((a) and (b)) and 9 rats in the MK801 treatment group ((c) and (d)) during the 80 trials of set 2. Dark gray and light gray squares indicate correct and incorrect responses, respectively. Each row gives the responses of a different animal and each column represents a different trial. Both groups were trained to discriminate one of the categories of the brightness dimension in set 1. Parts (a) and (b) are the respective responses of the 6 vehicle rats that were rewarded for entering the lighter (darker) arm in set 1. Parts (c) and (d) are the respective responses of the 3 (6) treatment rats that were rewarded for entering the lighter (darker) arm in set 1. White squares indicate the 8-CCR (consecutive correct response) learning trial estimate of the learning trial for each individual. Rats not achieving the 8-CCR criterion were assigned a learning trial of 80.

Source: Smith et al. (2005), *Journal of Neurophysiology*. Reprinted with permission, Copyright © 2005, American Physiological Association.

learning curve and to estimate the population learning curves for each of the four groups and to characterize the differences in learning between treatment and vehicle and between light and dark exposure on the previous day (Figure 6.10). The analysis with the population learning model shows that the two treatment groups had impaired learning (trials of 29 and 44) relative to the two vehicle groups (11 and 29). It also shows that the light exposure groups had more rapid learning (trials 11 and 29) compared with trials 30 and 44 for the dark exposure groups.

These results are consistent with the expected effect of MK801 on task acquisition and with expected behaviors of rats exposed to light and dark environments. Furthermore, they demonstrate the benefits of a hierarchical

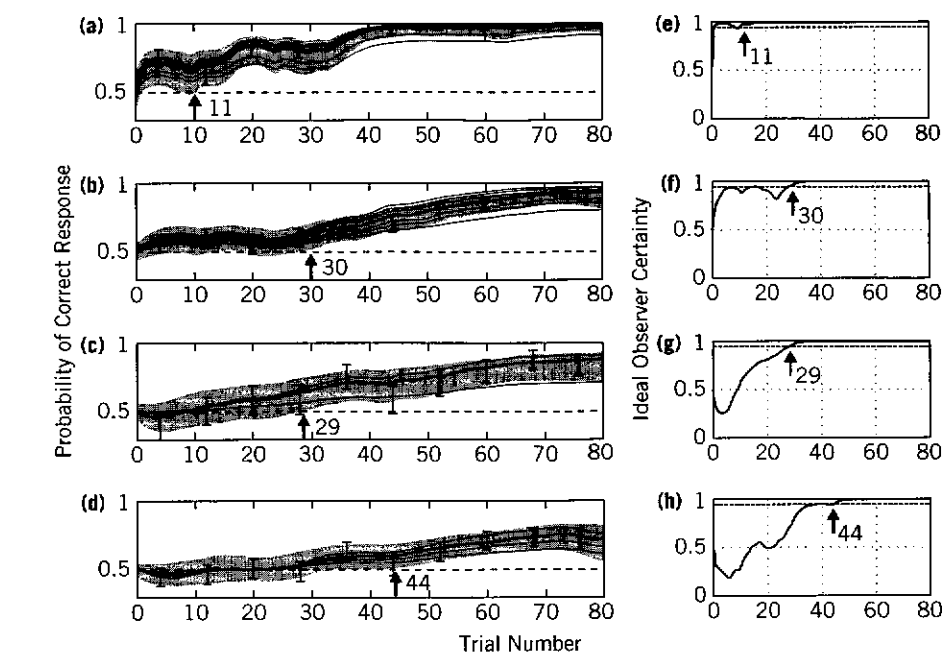


FIGURE 6.10

State space random effects (SSRE) estimation of population and individual learning. Population learning curves (dark gray) for the vehicle light (a), vehicle dark (b), treatment light (c), and treatment dark (d) subgroups and the associated 90% confidence intervals (light gray shaded area). Medium gray curves are the individual SSRE learning curves in each subgroup. Black error bars are the learning curve estimates from the 8-TB method \pm SE. Arrows indicate the respective ideal observer (IO(0.95)) learning trials. Ideal observer curves (dark gray) for the vehicle light (e), vehicle dark (f), treatment light (g), and treatment dark subgroups (h). All of the ideal observer curves (dark gray) start at 0.5, the probability of a correct response by chance. The trial where an ideal observer curve crosses and stays above 0.95 (dashed horizontal line) is the IO(0.95) learning trial for that group. Please see this figure in color at the companion web site: www.elsevierdirect.com/companions/9780123750273

Source: Smith et al. (2005), *Journal of Neurophysiology*, Reprinted with permission, Copyright © 2005, American Physiological Association.

model for simultaneously characterizing individual and population learning dynamically with a single analysis.

6.4 DISCUSSION

An important objective of neuroscience data analysis is the development of statistical techniques to characterize the dynamic features inherent in

most neuroscience data. State space models provide a tractable and flexible statistical framework for dynamic modeling. The estimation strategies chosen depend on the state space and observational model characteristics. We reviewed the state space paradigm with point process and binary observation models by discussing its application to the analysis of neural spike train and behavioral data. We considered the problems of neural spike train decoding, characterizing neural plasticity, analyses of behavior learning experiments, and the estimation of cortical neuronal UP/DOWN states. We conducted simultaneous state and parameter estimation using maximum likelihood methods implemented with EM algorithms in which Gaussian approximations and Monte Carlo methods were used to carry out the E-steps.

We reviewed only a small number of state space modeling applications in neuroscience. State space modeling has been applied to a variety of neural data analyses, including

- Analysis of between-trial and within-trial neural spiking dynamics (Czanner et al., 2008)
- Analysis of time-varying high-order correlations among simultaneously recorded neural spike trains (Shimazaki et al., 2009)
- Estimation of spike rate functions (Smith et al., 2010)
- Design of algorithms for control of neural prosthetic devices (Wu et al., 2006; Srinivasan et al., 2006, 2007; Hatsopoulos and Donoghue, 2009)
- Solving inverse problems for either functional imaging (Penny et al., 2005) or multi-channel EEG or MEG recordings (Barton et al., 2009; Lamus et al., 2010)

State space models have also been used to analyze calcium imaging (Vogelstein et al., 2009), to decode biophysical recordings (Huys and Paninski, 2009; Paninski, 2009), and to conduct causality analyses (Wong and Ozaki, 2007).

There are several important future directions in which the state space modeling paradigm can be extended. First, maximum likelihood algorithms have obvious Bayesian extensions. Extensions for the analysis of behavioral data can be easily implemented using standard software (Smith et al., 2007). In general, the development of computationally efficient estimation algorithms for the analysis of large-scale neuroscience data (Long et al., 2006; Ahmadian et al., 2009; Koyama and Paninski, 2009; Paninski et al., 2009; Koyama et al., 2010a,b) is another important direction. Second, the observation models can be extended to include mixed (continuous, point process, and binary) observation models for multimodal neural data that are recorded on the same or

different time scales. For example, a state and parameter estimation algorithm was recently developed for cognitive state estimation from simultaneously recorded continuous and binary measures of performance (Prerau et al., 2008; Prerau et al., 2009). Finally, the development of state space models to handle state switching (Kim and Nelson, 1999; Ghahramani and Hinton, 2000; Wu et al., 2004; Srinivasan et al., 2007; Fox et al., 2009) and hierarchical state space models (Ghahramani, 1998; Friston, 2008) for neuroscience applications is another important direction. All of these can be treated within the unifying framework of graphical models (Jordan, 1997; Airoldi, 2007).

Acknowledgments

This work was supported by NIH grants R01-DA015644, R01-MH071847, and R01-HL084502, and by NIH Director Pioneer Award DP1-OD003646.

References

- Ahmadian, Y., Pillow, J., Paninski, L., 2009. Efficient Markov chain Monte Carlo methods for decoding neural spike trains. Submitted.
- Airoldi, E.M., 2007. Getting started in probabilistic graphical models. *PLoS Comput. Biol.* 3 (12), e252.
- Barbieri, R., Frank, L.M., Nguyen, D.P., Quirk, M.C., Solo, V., Wilson, M.A., et al., 2004. Dynamic analyses of information encoding by neural ensembles. *Neural Comput.* 16, 277–307.
- Barton, M.J., Robinson, P.A., Kumar, S., Galka, A., Durrant-Whyte, H.F., Guivant, J., et al., 2009. Evaluating the performance of Kalman-filter-based EEG source localization. *IEEE Trans. Biomed. Eng.* 56, 122–136.
- Barnes, T.D., Kubota, Y., Hu, D., Jin, D.Z.Z., Graybiel, A.M., 2005. Activity of striatal neurons reflects dynamic encoding and recoding of procedural memories. *Nature* 437, 1158–1161.
- Battaglia, F.P., Sutherland, G.R., McNaughton, B.L., 2004. Hippocampal sharp wave bursts coincide with neocortical “up-state” transitions. *Learn. Mem.* 11, 697–704.
- Bialek, W., Rieke, F., de Ruyter van Steveninck, R.R., Warland, D., 1991. Reading a neural code. *Science* 252, 1854–1857.
- Boas, D.A., Brooks, D.H., Miller, E.L., DiMarzio, C.A., Kilmer, M., Gaudette, R.J., et al., 2001. Imaging the body with diffuse optical tomography. *IEEE Signal Process. Mag.* 18, 57–75.
- Brockwell, A.E., Rojas, A.L., Kass, R.E., 2004. Recursive Bayesian decoding of motor cortical signals by particle filtering. *J. Neurophysiol.* 91, 1899–1907.
- Brockwell, A.E., Kass, R.E., Schwartz, A.B., 2007. Statistical signal processing and the motor cortex. *Proc. IEEE* 95, 881–898.
- Brooks, S., Gelman, A., 1998. General methods for monitoring convergence of iterative simulations. *J. Comput. Graph. Stat.* 7, 434–455.

- Brown, E.N., 2005. The theory of point processes for neural systems. In: Chow, C.C., Gutkin, B., Hansel, D., Meunier, C., Dalibard, J. (Eds.), *Methods and Models in Neurophysics*. Elsevier, Paris, pp. 691–726.
- Brown, E.N., Barbieri, R., Eden, U.T., Frank, L.M., 2003. Likelihood methods for neural data analysis. In: Feng, J. (Ed.), *Computational Neuroscience: A Comprehensive Approach*. CRC Press, London, pp. 253–286.
- Brown, E.N., Barbieri, R., Ventura, V., Kass, R.E., Frank, L.M., 2002. The time-rescaling theorem and its application to neural spike data analysis. *Neural Comput.* 14, 325–346.
- Brown, E.N., Frank, L.M., Tang, D., Quirk, M.C., Wilson, M.A., 1998. A statistical paradigm for neural spike train decoding applied to position prediction from ensemble firing patterns of rat hippocampal place cells. *J. Neurosci.* 18, 7411–7425.
- Brown, E.N., Mitra, P.P., Kass, R.E., 2004. Multiple neural spike train data analysis: state-of-the-art and future challenges. *Nat. Neurosci.* 7, 456–461.
- Brown, E.N., Nguyen, D.P., Frank, L.M., Wilson, M.A., Solo, V., 2001. An analysis of neural receptive field plasticity by point process adaptive filtering. *Proc. Natl. Acad. Sci.* 98, 12261–12266.
- Cappé, O., Moulines, E., Rydén, T., 2005. *Inference in Hidden Markov models*. Springer, Berlin.
- Cappé, O., Godsill, S.J., Moulines, E., 2007. An overview of existing methods and recent advances in sequential Monte Carlo. *Proc. IEEE* 95 (5), 899–924.
- Carlin, B.P., Polson, N.G., Stoffer, D.S., 1992. A Monte Carlo approach to nonnormal and nonlinear state-space modeling. *J. Am. Stat. Assoc.* 87, 493–500.
- Chan, K.S., Ledolter, J., 1995. Monte Carlo EM estimation for time series models involving counts. *J. Am. Stat. Assoc.* 90, 242–252.
- Chen, Z., Vijayan, S., Barbieri, R., Wilson, M.A., Brown, E.N., 2009. Discrete-and continuous-time probabilistic models and algorithms for inferring neuronal UP and DOWN states. *Neural Comput.* 21, 1797–1862.
- Czanner, G., Eden, U.T., Wirth, S., Yanike, M., Suzuki, W.A., Brown, E.N., 2008. Analysis of between-trial and within-trial neural spiking dynamics. *J. Neurophysiol.* 99, 2672–2693.
- Daley, D., Vere-Jones, D., 2002. *An Introduction to the Theory of Point Processes*, Vol. 1: Elementary Theory and Methods. Springer, New York.
- deJong, P., MacKinnon, M.J., 1988. Covariances for smoothed estimates in state space models. *Biometrika* 75, 601–602.
- Dempster, A., Laird, N., Rubin, D.B., 1977. Maximum likelihood from incomplete data via the EM algorithm. *J. R. Stat. Soc. B* 39, 1–38.
- Denk, W., Strickler, J.H., Webb, W.W., 1990. Two-photon laser scanning fluorescence microscopy. *Science* 248, 73–76.
- Djuric, P., 2001. Sequential estimation of signals under model uncertainty. In: *Sequential Monte Carlo Methods in Practice*. Springer, New York.
- Doucet, A., de Freitas, N., Gordon, N., 2001. *Sequential Monte Carlo Methods in Practice*. Springer, New York.
- Durbin, J., Koopman, S.J., 2001. *Time Series Analysis by State Space Methods*. Oxford Univ. Press.
- Eden, U.T., Frank, L.M., Barbieri, R., Solo, V., Brown, E.N., 2004. Dynamic analyses of neural encoding by point process adaptive filtering. *Neural Comput.* 16, 971–998.
- Eden, U.T., Brown, E.N., 2008. Continuous-time filters for state estimation from point process models of neural data. *Stat. Sin.* 18, 1293–1310.
- Ergun, A., Barbieri, R., Eden, U.T., Wilson, M.A., Brown, E.N., 2007. Construction of point process adaptive filter algorithms for neural systems using sequential Monte Carlo methods. *IEEE Trans. Biomed. Eng.* 54 (3), 419–428.
- Fahrmeir, L., Tutz, G., 2001. *Multivariate Statistical Modelling Based on Generalized Linear Models*, second ed. Springer, New York.
- Fox, E.L., Sudderth, E.B., Jordan, M.I., Willsky, A.S., 2009. Nonparametric Bayesian learning of switching linear dynamical systems. In: *Advances in Neural Information Processing Systems 22*. MIT Press, Cambridge, MA.
- Frank, L.M., Stanley, G.B., Brown, E.N., 2004. Hippocampal plasticity across multiple days of exposure to novel environments. *J. Neurosci.* 24, 7681–7689.
- Friston, K., 2008. Hierarchical models in the brain. *PLoS Comput. Biol.* 4 (11), e1000211. doi:10.1371/journal.pcbi.1000211.
- Gelman, A., Carlin, J.B., Stern, H.S., Rubin, D.B., 2004. *Bayesian Data Analysis*, second ed. Chapman & Hall/CRC, Boca Raton, FL.
- Ghahramani, Z., 1998. Learning dynamic Bayesian networks. In: Giles, C.L., Gori, M. (Eds.), *Adaptive Processing of Sequences and Data Structures*. Springer-Verlag, Berlin, pp. 168–197.
- Ghahramani, Z., Hinton, G.E., 2000. Variational learning for switching state-space models. *Neural Comput.* 12, 831–864.
- Gilks, W.R., Richardson, S., Spiegelhalter, D.J., 1996. *Markov Chain Monte Carlo in Practice*. Chapman & Hall/CRC Press, Boca Raton, FL.
- Green, P.J., 1995. Reversible jump Markov chain Monte Carlo computation and Bayesian model determination. *Biometrika* 82, 711–732.
- Haider, B., Duque, A., Hasenstaub, A.R., Yu, Y., McCormick, D.A., 2007. Enhancement of visual responsiveness by spontaneous local network activity in vivo. *J. Neurophysiol.* 97, 4186–4202.
- Hämäläinen, M., Hari, R., Ilmoniemi, R., Knuutila, J., Lounasmaa, O., 1993. Magnetoencephalography—theory, instrumentation, and applications to noninvasive studies of the working human brain. *Rev. Mod. Phys.* 65, 1–93.
- Hatsopoulos, N.G., Donoghue, J.P., 2009. The science of neural interface systems. *Annu. Rev. Neurosci.* 32, 249–266.
- Haykin, S., 2002. *Adaptive Filter Theory*, fourth ed. Prentice Hall, Upper Saddle River, NJ.
- Hochberg, L.R., Serruya, M.D., Friehs, G.M., Mukand, J.A., Saleh, M., Caplan, A.H., et al., 2006. Neuronal ensemble control of prosthetic devices by a human with tetraplegia. *Nature* 442, 164–171.
- Huys, Q.J.M., Paninski, L., 2009. Smoothing of, and parameter estimation from, noisy biophysical recordings. *PLoS Comput. Biol.* 5 (5), e1000379.
- Ji, D., Wilson, M.A., 2007. Coordinated memory replay in the visual cortex and hippocampus during sleep. *Nature Neurosci.* 10, 100–107.
- Jog, M.S., Kubota, Y., Connolly, C.I., Hillegaart, V., Graybiel, A.M., 1999. Building neural representations of habits. *Science* 286, 1745–1749.
- Jones, R.H., 1993. *Longitudinal Data with Serial Correlation: A State-Space Approach*. Chapman & Hall, New York.
- Jordan, M.I. (Ed.), 1997. *Learning in Graphical Models*. MIT Press, Cambridge, MA.
- Kim, C.-J., Nelson, C.R., 1999. *State-Space Models with Regime Switching: Classical and Gibbs-Sampling Approaches with Applications*. MIT Press, Cambridge, MA.

- Kitagawa, G., Gersh, W., 1996. Smoothness Priors Analysis of Time Series. Springer, New York.
- Koyama, S., Paninski, L., 2009. Efficient computation of the maximum a posteriori path and parameter estimation in integrate-and-fire and more general state-space models. *J. Comput. Neurosci.* (in press).
- Koyama, S., Eden, U.T., Brown, E.N., Kass, R.E., 2010a. Bayesian decoding of neural spike trains. *Ann. Inst. Stat. Math.* 62, 37–59.
- Koyama, S., Perez-Bolde, L.C., Shalizi, C.R., Kass, R.E., 2010b. Approximate methods for state-space models. *J. Amer. Stat. Assoc.* 105, 170–180.
- Kwong, K.K., Belliveau, J.W., Chesler, D.A., Goldberg, I.E., Weisskoff, R.M., Poncelet, B.P., et al., 1992. Dynamic magnetic resonance imaging of human brain activity during primary sensory stimulation. *Proc. Natl. Acad. Sci. U.S.A.* 89, 5675–5679.
- Lamus, C., Hamalainen, M.S., Temereanca, S., Brown, E.N., Purdon, P.L., 2010. How dynamic models of brain connectivity can help solve the MEG inverse problem: analysis of source observability. Submitted.
- Law, J.R., Flanery, M.A., Wirth, S., Yanike, M., Smith, A.C., Frank, L.M., et al., 2005. Functional magnetic resonance imaging activity during the gradual acquisition and expression of paired-associate memory. *J. Neurosci.* 25, 5720–5729.
- Long, C.J., Desai, N.U., Hämäläinen, M., Temereanca, S., Purdon, P.L., Brown, E.N., 2006. A dynamic solution to the ill-conditioned magnetoencephalography (MEG) source localization problem. In: Proc. ISBI'06, 225–228.
- McLachlan, G.J., Krishnan, T., 2008. The EM Algorithm and Extensions, second ed. Wiley, New York.
- Mendel, J.M., 1995. Lessons in Estimation Theory for Signal Processing, Communication, and Control. Prentice Hall, Upper Saddle River, NJ.
- Moran, D.W., Schwartz, A.B., 1999. Motor cortical representation of speed and direction during reaching. *J. Neurophysiol.* 82, 2676–2692.
- Musallam, S., Corneil, B.D., Greger, B., Scherberger, H., Andersen, R.A., 2004. Cognitive control signals for neural prosthetics. *Science* 305, 258–262.
- Okatan, M., Wilson, M.A., Brown, E.N., 2005. Analyzing functional connectivity using a network likelihood model of ensemble neural spiking activity. *Neural Comput.* 17, 1927–1961.
- Ogawa, S., Tank, D.W., Menon, R., Ellermann, J.M., Kim, S.G., Merkle, H., et al., 1992. Intrinsic signal changes accompanying sensory stimulation: functional brain mapping with magnetic resonance imaging. *Proc. Natl. Acad. Sci. U.S.A.* 89, 5951–5955.
- Paninski, L., 2009. Inferring synaptic inputs given a noisy voltage trace via sequential Monte Carlo methods. *J. Comput. Neurosci.* Submitted.
- Paninski, L., Ahmadian, Y., Ferreira, D., Koyama, S., Rahnama, K., Vidne, M., et al., 2009. A new look at state-space models for neural data. *J. Comput. Neurosci.* (in press).
- Pawitan, Y., 2001. In All Likelihood: Statistical Modelling and Inference Using Likelihood. Clarendon Press, Oxford, UK.
- Penny, W., Ghahramani, Z., Friston, K., 2005. Bilinear dynamical systems. *Philos. Trans. R. Soc. Lond. B* 360, 983–993.
- Prerau, M., Smith, A.C., Eden, U.T., Yanike, M., Suzuki, W.A., Brown, E.N., 2008. A mixed filter algorithm for cognitive state estimation from simultaneously recorded continuous and binary measures of performance. *Biol. Cybern.* 99, 1–14.
- Prerau, M., Smith, A.C., Eden, U.T., Kubota, Y., Yanike, M., Suzuki, W., et al., 2009. Characterizing learning by simultaneous analysis of continuous and binary measures of performance. *J. Neurophysiol.* 102, 3060–3072.
- Rieke, F., Warland, D., de Ruyter van Steveninck, R.R., Bialek, W., 1997. Spikes: Exploring the Neural Code. MIT Press, Cambridge, MA.
- Robert, C.P., Casella, G., 2004. Monte Carlo Statistical Methods, second ed. Springer-Verlag, New York.
- Roweis, S., Ghahramani, Z., 1999. A unifying review of linear Gaussian models. *Neural Comput.* 11, 305–345.
- Santhanam, G., Ryu, S.I., Yu, B.M., Afshar, A., Shenoy, K.V., 2006. A high-performance brain-computer interface. *Nature* 442, 195–198.
- Serruya, M.D., Hatsopoulos, N.G., Paninski, L., Fellows, M.R., Donoghue, J.P., 2002. Instant neural control of a movement signal. *Nature* 416, 141–142.
- Shephard, N., Pitt, M.K., 1997. Likelihood analysis of non-Gaussian measurement time series, *Biometrika*, 84, 653–667.
- Shimazaki, H., Amari, S., Brown, E.N., Gruen, S., 2009. State-space analysis on time-varying correlations in parallel spike sequences. In: Proc. IEEE ICASSP (pp. 3501–3504), Taipei.
- Shumway, R.H., Stoffer, D.S., 1982. An approach to time series smoothing and forecasting using the EM algorithm. *J. Time Ser. Anal.* 3, 253–264.
- Shoham, S., Paninski, L.M., Fellows, M.R., Donoghue, J.P., Normann, R.A., 2005. Statistical encoding model for a primary motor cortical brain-machine interface. *IEEE Trans. Biomed. Eng.* 52, 1312–1322.
- Smith, A.C., Brown, E.N., 2003. Estimating a state-space model from point process observations. *Neural Comput.* 15, 965–991.
- Smith, A.C., Frank, L.M., Wirth, S., Yanike, M., Hu, D., Kubota, Y., et al., 2004. Dynamical analysis of learning in behavior experiments. *J. Neurosci.* 24, 447–461.
- Smith, A.C., Stefani, M.R., Moghaddam, B., Brown, E.N., 2005. Analysis and design of behavioral experiments to characterize population learning. *J. Neurophysiol.* 93, 776–792.
- Smith, A.C., Wirth, S., Suzuki, W., Brown, E.N., 2007. Bayesian analysis of interleaved learning and response bias in behavioral experiments. *J. Neurophysiol.* 97, 2516–2524.
- Smith, A.C., Scalon, J., Wirth, S., Yanike, M., Suzuki, W., Brown, E.N., 2010. State-space algorithms for estimating spike rate functions. *J. Comput. Intell. Neurosci.* Online publication Article ID 426539. doi: 10.1155/2010/426539
- Spall, J.C., 2003. Estimation via Markov chain Monte Carlo. *IEEE Control Syst. Mag.* 23 (2), 34–45.
- Srinivasan, L., Eden, U.T., Willsky, A.S., Brown, E.N., 2006. A state-space analysis for reconstruction of goal-directed movements using neural signals. *Neural Comput.* 18, 2465–2494.
- Srinivasan, L., Brown, E.N., 2007. A state-space framework for movement control to dynamic goals through brain-driven interfaces. *IEEE Trans. Biomed. Eng.* 54 (3), 526–535.

- Srinivasan, L., Eden, U.T., Mitter, S.K., Brown, E.N., 2007. General-purpose filter design for neural prosthetic devices. *J. Neurophysiol.* 98, 2456–2475.
- Stanley, G.B., Li, F.F., Dan, Y., 1999. Reconstruction of natural scenes from ensemble responses in the LGN. *J. Neurosci.* 19, 8036–8042.
- Suzuki, W.A., Brown, E.N., 2005. Behavior and neurophysiological analyses of dynamic learning processes. *Behav. Cogn. Neurosci. Rev.* 4, 67–95.
- Tanner, M.A., 1996. Tools for Statistical Inference, third ed. Springer, New York.
- Taylor, D.M., Tillery, S.I.H., Schwartz, A.B., 2002. Direct cortical control of 3D neuroprosthetic devices. *Science* 296, 1829–1832.
- Truccolo, W., Eden, U.T., Fellow, M., Donoghue, J.D., Brown, E.N., 2005. A point process framework for relating neural spiking activity to spiking history, neural ensemble and covariate effects. *J. Neurophysiol.* 93, 1074–1089.
- Vogelstein, J., Watson, B., Packer, A., Yuste, R., Jedynak, B., Paninski, L., 2009. Spike inference from calcium imaging using sequential Monte Carlo methods. *Biophys. J.* 97, 636–655.
- Wilson, M.A., McNaughton, B.L., 1993. Dynamics of the hippocampal ensemble code for space. *Science* 261, 1055–1058.
- Wilson, M.A., McNaughton, B.L., 1994. Reactivation of hippocampal ensemble memories during sleep. *Science* 265, 676–679.
- Wirth, S., Yanike, M., Frank, L.M., Smith, A.C., Brown, E.N., Suzuki, W.A., 2003. Single neurons in the monkey hippocampus and learning of new associations. *Science* 300, 1578–1584.
- Wong, K.F.K., Ozaki, T., 2007. Akaike causality in state space: instantaneous causality between visual cortex in fMRI time series. *Biol. Cybern.* 97, 151–157.
- Wu, W., Black, M.J., Mumford, D., Gao, Y., Bienenstock, E., Donoghue, J.P., 2004. Modeling and decoding motor cortical activity using a switching Kalman filter. *IEEE Trans. Biomed. Eng.* 51, 933–942.
- Wu, W., Gao, Y., Bienenstock, E., Donoghue, J.P., Black, M.J., 2006. Bayesian population decoding of motor cortical activity using a Kalman filter. *Neural Comput.* 18, 80–118.
- Wu, W., Kulkarni, J.E., Hatsopoulos, N.G., Paninski, L., 2009. Neural decoding of hand motion using a linear state-space model with hidden states. *IEEE Trans. Neural Syst. Rehabil. Eng.* 17, 370–378.
- Zhang, K., Ginzburg, I., McNaughton, B.L., Sejnowski, T.J., 1998. Interpreting neuronal population activity by reconstruction: unified framework with application to hippocampal place cells. *J. Neurophysiol.* 79, 1017–1044.